Decoding human placental cellular and molecular responses to obesity and fetal growth

Hong Jiang[1†], Emilie Derisoud[1†], Denise Parreira[2], Nayere Taebnia[1,3], Paulo R. Jannig[1], Reza Zandi Shafagh[1,3,6], Allan Zhao[1], Congru Li[1], Macarena Ortiz[5], Manuel Alejandro Maliqueo[5], Elisabet Stener-Victorin[1], Volker M. Lauschke[1,3,4,7], Qiaolin Deng[1,2,*]

[1]Karolinska Institutet, Department of Physiology and Pharmacology, Stockholm, 17177, Sweden

[2]Stockholm University, Department of Molecular Biosciences, the Wenner-Gren Institute, 10691, Sweden

[3]Center for Molecular Medicine, Karolinska Institutet and University Hospital, Stockholm, 17176 Sweden

[4]Dr Margarete Fischer-Bosch Institute of Clinical Pharmacology, Stuttgart, 70376, Germany

[5]University of Chile, Departamento de Medicina Interna, Santiago, 8330015, Chile

[6]Division of Micro- and Nanosystems, KTH Royal Institute of Technology, Stockholm, Sweden

[7]Department of Pharmacy, the Second Xiangya Hospital, Central South University, Changsha, China

[†] These authors have contributed equally to this work and share first authorship

* Corresponding Author: qiaolin.deng@ki.se (ORCID ID: 0000-0001-5934-7816)

Abstract

Maternal obesity increases risk of large-for-gestational-age (LGA) births and subsequent cardiometabolic disorders in offspring. To identify placental signatures associated with these outcomes, we performed single-nucleus RNAseq on placentas from women with obesity delivering appropriate-for-gestational-age (AGA) or LGA infants, compared to normal-weight controls. In maternal obesity, regardless of fetal growth, syncytiotrophoblasts showed upregulated hypoxia and TNF-α signaling, while cytotrophoblasts exhibited downregulated receptor tyrosine kinase signaling. However, only in LGA placentas, villous non-trophoblasts displayed upregulated TNF-α signaling and inflammatory responses. Notably, Hofbauer cells in LGA placentas presented transcriptional alterations in immunometabolism-related genes and functioned as main signaling senders via *SPP1*. Importantly, we recapitulated syncytiotrophoblast responses to maternal obesity using a novel microfluidic organoids-on-a-chip co-culture. These findings reveal distinct transcriptional responses of placental cell types to maternal obesity and fetal growth, highlighting potential intervention pathways to mitigate future disease risks.

Introduction

The global prevalence of obesity among women of reproductive age reached 18.5% in 2022, making maternal obesity an increasing concern for women's health (*1*). Maternal obesity is manifested by chronic low-grade inflammation, hyperinsulinemia, and dysregulated lipid metabolism (*2*). Consequently, these systemic changes collectively impact the intrauterine environment and lead to immediate and long-term health consequences for both mothers and their offspring including greater risk to develop cardiometabolic diseases and type 2 diabetes (*3-5*). Among pregnancy complications, delivery of large-for-gestational-age (LGA) infants (birthweight > 90th percentile (*6*)) is one of the most frequently observed ones, occurring in 13.41%-38.3% of pregnancies affected by obesity (*7-10*). Notably, LGA itself is not only a pregnancy complication but also a critical risk factor for further adverse outcomes, including birth trauma (*11*), childhood obesity (*12*), cardiometabolic and neurological disorders in early adulthood (*13*). Therefore, preventing LGA may serve as an effective strategy to mitigate the cascade of associated complications.

Maternal obesity is often associated with excessive gestational weight gain (*14*), which subsequently contributes to a higher risk of LGA infants due to excess nutrient supply (*15*). However, the UK UPBEAT study, a randomized controlled trial testing a tailored complex lifestyle intervention (diet and physical activity) in pregnant women with obesity, found that reduction in gestational weight gain did not have significant effects on the outcomes of gestational diabetes and LGA infants (*16*). Also, the EMPOWaR study found that pharmacological use of metformin in pregnant women with obesity had no significant effect on reducing birthweight percentiles or preventing adverse neonatal outcomes despite clearly improving maternal metabolic health (*17*). These studies collectively pinpoint the potential additional mechanisms contributing to fetal growth, and lack of success in preventing LGA infants with current interventions hence underscores the need for a deeper understanding of the underlying mechanisms.

Intriguingly, not all fetuses exposed to maternal obesity exhibit excessive growth and develop LGA, with some still following a normative growth trajectory resulting in AGA. This intrinsic variability may reflect an inherent adaptive mechanism *in utero* that could be harnessed for future LGA management. The placenta is the central structure at the maternal-fetal interface, regulating the quantity and quality of nutrient supply from the maternal circulation by adjusting its transport capacity and nutrient uptake (*18*). Additionally, it dynamically modulates growth factors and hormonal secretion (*19*) and adjusts inflammation levels (*20*) to align with the growth requirements of the fetus. These activities are intertwined and could serve as the link between maternal obesity and divergent fetal growth trajectories. For example, elevated maternal insulin levels in obesity activate mTOR signaling as well as glucose and amino acid transport in the placenta, thus contributing to accelerated fetal growth in some women with obesity (*21*). Circulating pro-inflammatory cytokines in obesity, such as IL-6, tumor necrosis factor-α (TNF-α) and leptin are found to promote lipid storage in the placenta (*20*) and enhance amino acid and lipid transporters in trophoblast. Moreover, secretion of placental lactogen and prolactin are correlated with pre-pregnancy BMI and fetal growth (*22*), further supporting the active role of the placenta in modulating the effects of obesity on fetal growth (*23*).

However, current understanding of the placental response to maternal obesity largely relies on gene expression analyses conducted at the whole-tissue level or in cell cultures (*24-27*), which are often confounded by tissue complexity or lack of physiological relevance in culture conditions. Therefore, identifying molecular signatures in the placenta associated with AGA and LGA infants at a single-cell level may provide valuable insights into cell-type specific mechanisms driving distinct growth patterns and inform potential targeted therapeutic strategies. Here, we performed single-nucleus RNAseq (snRNA-seq) on term placentas collected in a Chilean cohort study, in which women with obesity that did not develop other pregnancy complications except for more frequent delivery of LGA infants (*28*). We divided the placental samples and analyzed three groups: normal BMI with AGA infants (Control), maternal obesity with AGA infants (O-A), and maternal obesity with LGA infants (O-L). Cell-type specific transcriptomic profiles and pathways were identified to be either share or different in O-A and O-L groups, suggesting molecular responses to maternal obesity or fetal growth, respectively. Moreover, the intercellular ligand-receptor communication network revealed the major cell types mediating these maternal or fetal effects. Finally, microfluidic co-culture of adipose spheroids and trophoblast organoids could recapitulate some transcriptional changes of trophoblasts in maternal obesity, providing an *in vitro* model with mechanistic insights to study the effects of maternal conditions on human placentas in future.

Results

Cell types in placentas stratified by maternal obesity and fetal growth

To analyze the placental transcriptional changes in maternal obesity and investigate the interplay between the placenta and fetal overgrowth, we selected 12 samples from a birth cohort with representative maternal BMI and birthweights for snRNA-seq (*28*) (Fig. 1A and fig. S1A). All samples were from vaginal delivery and the O-A and O-L groups had no significant differences in maternal age, placental weight and placental efficiency compared with Controls (Fig. 1B, Fig. 1A). We dissected the placental villous region and dissociated the tissue into single nuclei, followed by library preparation using 10x Chromium (Fig. 1C). A total of 37,408 nuclei were retained for downstream analyses after stringent quality control, yielding comparable total counts and gene number per cell across all groups (Fig. 1D). Using canonical marker genes for cell types (*29*), we

annotated 14 placental cell types, including five types of trophoblasts, two states of endothelial cells, two types of fibroblasts, and five types of leukocytes (Fig. 1E). There was no significant difference in the proportion of cell types, either in various trophoblasts or in different villous non-trophoblast cells, across the three groups (Fig. 1F, G and Appendix Table S1).

Trophoblasts comprised the majority of cells, primarily syncytiotrophoblast (STB) and villous cytotrophoblasts (CTBs). Proliferative CTBs (pCTBs) were identified as being in the cell cycle (Fig. 1H, fig. S1B). Co-expression of *ERVW-1* (Syncytin-1) and *ERVFRD-1* (Syncytin-2) identified early STB (eSTB), consistent with previous findings (*30*). Mature STB shared expression of *ERVW-1* and *CYP19A1* with eSTB but uniquely expressed *CSH1* and *PSG3* (Fig. 1H). The extravillous trophoblasts (EVTs) accounted for only 0.5% of all nuclei, with fewer than one hundred per group, aligning with our villous sampling approach (Appendix Table S1). Among other villous non-trophoblast cells, stromal cells within the chorionic villi included fibroblasts and myofibroblasts. Myofibroblasts were annotated by concurrently expressing collagen (*COL3A1* and *COL1A1*), actin (*ACTA2*) and myosin subunits (*MYH11*) (Fig. 1H). Vascular endothelial cells (VECs) were divided into a small subset of $GJA5^{+}$ and $GJA5^{-}$ VEC (Fig. 1H and fig. S1C). *GJA5* is a gap junction protein facilitating direct intercellular communication by forming channels. Among the immune cells, we primarily captured Hofbauer cells, specialized macrophages located within the chorionic villi (Fig. 1H). *PTPRC* was also detected in other remaining nuclei, indicating their leukocyte origin. These remaining nuclei could be further annotated into monocyte, B cells, NK cells and T cells (Fig. 1H and Appendix Table S1). However, due to their limited numbers (fig. S1D), likely carried over from dissection, and being outside the scope of our study, these cells were excluded from subsequent analyses.

Next, we focused on the major villous cell types, i.e., STB, CTB, VEC, fibroblasts and Hofbauer cells, to understand their distinct molecular signatures in the placental responses to obesity and regulation of fetal growth. To identify functional pathways and gene expression changes in each cell type, we developed a scoring (C-score) metric to quantitatively measure the transcriptional changes in the two obesity groups, O-A and O-L compared to the control. The C-score metric was calculated based on the effect size and the false discovery rate from differential gene expression analysis and gene set enrichment analysis followed by ranking. A high positive C-score indicated maternal effects independent of fetal overgrowth, as these genes and pathways were similarly regulated in both comparisons (i.e., O-A vs. control and O-L vs. control). In contrast, a low negative C-score indicated effects linked to fetal growth effects, as the O-A and O-L groups exhibited different changes (see Methods: Scoring the shared or different DEGs between comparisons). This method provided a systematic approach to rank changes due to maternal or fetal growth effects across all cell types and cell-cell communications in the placenta, without relying on arbitrary fold-change cutoffs. The number of the shared or different DEGs was provided in Appendix Table S2.

Identification of STB subpopulations along the maturation states

The STB layer is formed through the fusion of CTBs, a process that requires remodeling of cytoskeletal and plasma membrane dynamics. A total of 24,478 STB nuclei were captured, enabling us to investigate the subpopulations across the different phases of STB life cycle. We first re-clustered the STB nuclei and identified three substates (STB-a, -b and -c) (Fig. 2A). To better elucidate their maturation process, we incorporated CTBs and eSTBs as early differentiation timepoints to place STBs in context for pseudo-time analysis (fig. S2A). The three STB substates were aligned along the pseudo-time axis with varying numbers of cells distributed across the

timeline (Fig. 2B). Novel gene markers were subsequently identified, highlighting the biological differences among the substates (Fig. 2C and fig. S2B). STB-a appeared at an earlier stage characterized by the expression of *TENM3* (Fig. 2C, fig. S2C). *TENM3* encodes a teneurin transmembrane protein that promotes homophilic cellular adhesion (*31*). *TENM3*$^{+}$ STB was demonstrated in the STB layer by *in situ* hybridization (*32*). This state was also characterized by genes involved in cytoskeleton, tight junction, and extracellular matrix (*ITGB1*, collagen subunits *COL4A1, COL4A2*, *FN1* and *TIMP3*) (Fig. 2C). Furthermore, STB-b specifically expressed *PDE4D* (phosphodiesterase 4D), a cAMP-specific phosphodiesterases reported to limit over-syncytialization (*33*) (Fig. 2C). Finally, the mature STB-c state was characterized by the expression of tight junction inhibitors such as and *PKIB* (Fig. 2C, fig. S2C). *ADAMTS6* could inhibit cell-cell junctions and was previously identified as a marker of a distinct STB state (*34*, *35*). *PKIB* is involved in the cAMP pathway, crucial for STB formation (*33*). Accordingly, STB-b nuclei appeared to balance syncytialization, while STB-c nuclei actively engage in the process, collectively contributing to a dynamic balance. Excessive syncytialization leads to release of aged cytosolic material into maternal circulation, while restricted fusion results in exhaustion of the syncytial layer (*36*). Therefore, the dynamics of these three subpopulations may play a critical role in maintaining STB homeostasis. Reassuringly, these STB states were further confirmed and in line with previously identified various STB maturing substates by integrating our data with a recently published term placenta snRNA-seq dataset (*37*) using scANVI (*38*) (fig. S2D). The percentage of three STB states was not significantly different among three groups (Fig. 2D).

Transcriptional changes due to maternal or fetal growth effects among STB nuclei

The STB nuclei at different transcriptional states possibly varies in responses to surrounding signals. We first identify the underlying biological pathways in maternal obesity with or without fetal overgrowth utilized hallmark gene sets from MSigDB (*39*). Gene set enrichment analysis (GSEA) showed that O-A and O-L shared dysregulated pathways related to epithelial mesenchymal transition (EMT), apical junction and mitotic spindle regions in STB-a nuclei (Fig. 2E and Appendix Table S3). STB-b and STB-c also shared several dysregulated pathways in both groups, including complement, hypoxia, and TNF-α signaling via NF-kβ, all of which are indicative of inflammatory processes (Fig. 2E and Appendix Table S3). To determine genes within these pathways that may contribute to the pathways, we intersected shared and different DEGs with pathway-specific gene sets focusing on the hypoxia and TNF-α signaling in STB-b and STB-c (Fig. 2F). Among those shared genes driving the enrichment of the hypoxia signaling pathway, *FOXO3* and *FOS* have been reported as the crosstalk between hypoxia and TNF-α signaling (*40-43*). Important transporters such as *SLC2A1* (i.e. GLUT1) and *TFRC* may mediate the interaction between hypoxia, nutrient transfer and metabolism (*44, 45*) (Fig. 2G). *SLC2A1* is predominately expressed in the STB to facilitate glucose uptake from the maternal circulation and *TFRC* mediates cellular iron uptake. Expression of both is shown to be regulated by hypoxia (*45*).

Next, we used a previously published set of placenta-specific secreted proteins from the human secretome project (*46*). A total of 12 genes were identified being altered by maternal obesity, among which most were upregulated except for *CSHL1* (Fig. 2H). *CGA* encodes the alpha unit of human glycoprotein hormones, including hCG (chorionic gonadotropin). Changes in hCG levels have been linked to adverse pregnancy outcomes, and its dysregulation highlights the detrimental effects of maternal obesity on the placenta (*47*). A total of 5 genes encoding placenta-specific secreted proteins were identified to be regulated according to fetal growth. Specifically, *FBN2* was upregulated while *KISS1*, *PAPPA* and *CSH1* were downregulated in O-L (Fig. 2H). Notably, *FBN2* encodes placensin, a glucogenic hormone highly expressed in human placentas to stimulate hepatic

214 glucose secretion and cAMP production (*48*). It was elevated only in O-L but decreased in O-A, in
215 line with its increased expression in pregnancy complications such as gestational diabetes. *PAPPA*
216 encodes a metalloprotease secreted by the human placenta that modulates IGF bioavailability. Its
217 concentrations are inversely correlated with glycemia and odds of developing gestational diabetes
218 (*49*), aligning with our finding of the greatest reduction observed in the O-L group (Fig 2H). Such
219 different hormone regulation resulted from the placental responses to maternal uterine conditions
220 likely contributed to the different fetal growth effects.

221 Furthermore, the expression of receptors or channels that sense the maternal metabolic signals could
222 also be altered accordingly to fetal growth. We found that a total of 7 genes being altered differently
223 between O-A and O-L (Fig. 2I). Among those expressed in both STB-b and STB-c, *AHR* encodes
224 the aryl hydrocarbon receptor that senses the varied cellular environment, including endogenous
225 tryptophan derivatives, an essential amino acid critical for placental and fetal development (*50*).
226 *LIFR* encodes the receptor of leukemia inhibitory factor, and LIFR deficiency leads to impaired
227 placenta differentiation, reduced embryo viability, and increased birth weight in mice (*51*). *ANO2*
228 encodes a calcium-gated chloride channel and *CHSY1* is an enzyme for synthesis of chondroitin
229 sulfate in response to nutrient levels. All these genes were only upregulated in O-A but not in O-L,
230 suggesting an inadequate response in O-L (Fig. 2I).

231 *PI3K-AKT and MAPK cascade signaling pathways changes in CTBs*

232 Next, we analyzed the enrichment of hallmark gene sets in CTBs, the cell type that positions
233 beneath STB. In contrast to STB, the hallmark gene sets were we predominantly decreased in both
234 O-A and O-L (Appendix Table S3). These included apical junction, mitotic spindle, G2M
235 checkpoint, heme metabolism, hypoxia, IL2-STAT5 signaling (Fig. 3A). In contrast, Myc targets
236 showed a divergent response with downregulation only in O-L (Fig. 3A). MYC target pathway,
237 critical for CTB proliferation, differentiation, and metabolic adaptation, is often suppressed by
238 inflammation and hypoxia (*52*).

239 Next, we identified 102 genes as altered by maternal obesity in both O-A and O-L, among which
240 100 genes were downregulated genes (Fig 3B). Interestingly, the altered genes were significantly
241 enriched in the PI3K-Akt signaling pathway, with those highlighted in red specifically involved in
242 receptor tyrosine kinase (RTK)-mediated transduction of growth factor signals (Fig. 3C). In
243 addition, *HSP90AA1* is essential for stabilizing AKT activity, thereby facilitating the
244 phosphorylation and inactivation of FOXO3(*53*) (Fig. 3C). Among divergent genes, 15 and 9 genes
245 were downregulated in the O-A and O-L, respectively (Fig. 3B). Five of these dysregulated genes
246 (i.e., *WWC1, PRKCZ, MAPK4, KSR1, ERBB4)* are involved in enhancing the MAPK cascade
247 activation—a signaling pathway activated downstream of RTKs, similar to the PI3K-AKT pathway
248 (Fig. 3D). *ERBB4* encodes an EGFR, which belongs to RTKs, and was reported previously to be
249 expressed by CTB as a pro-survival factor under hypoxic conditions (*54*). Thus, our findings
250 suggest that in O-A, upregulation of the MAPK cascade might compensate for the downregulation
251 of the PI3K-Akt pathway, promoting downstream target expression, such as Myc targets (Fig. 3A,
252 E). However, this regulatory balance was likely absent in O-L, which could explain the observed
253 downregulation of Myc target genes in O-L (Fig. 3A). Altogether, the PI3K-Akt and MAPK
254 pathways, key downstream effectors of RTK signaling, are dysregulated in obesity and related to
255 fetal overgrowth.

256 *Transcriptional changes in non-trophoblast cell types due to maternal and fetal growth effects*

257 In VEC, most identified hallmark gene sets were downregulated in both O-A and O-L, including
258 gene sets related to complement signaling, G2M checkpoint, heme metabolism, IL2-STAT5
259 signaling, KRAS signaling and protein secretion (Fig. 4A). These pathways are related to immune
260 dysregulation, angiogenesis and metabolic stress, which have been shown as placental features of
261 maternal obesity (*55*). Further examining the dysregulated genes within these pathways identified
262 that 49 genes were altered by maternal obesity, and 3 genes were differently regulated in O-A and
263 O-L (Fig. 4B). 9 genes were reported to be critical for regulating VEGFA-VEGFR1 (i.e. FLT1)
264 signaling in angiogenesis (Fig. 4C). Among these, *GNA14, RAPGEF5, NRP1, COL4A2,* and
265 *COBLL1* have been reported to be co-expressed with *VEGFR1 (55)*, while *FN1* and *BMP6* have
266 synergistic effects on VEGFA complex (*56*) (Fig. 4C). The binding of VEGFA complex to
267 VEGFR1 promotes angiogenesis (*57*) and inflammatory cell recruitment (*58*), aligning with the
268 consequence of their dysregulation in maternal obesity. *NRP1* is an adaptor protein forming dimers
269 with VEGFA to bind VEGFR1 (*59*). *FN1* dysregulation has been shown to affect VEGFA
270 expression and relate to cellular apoptosis and autophagy in human umbilical vein endothelial cells
271 (*60, 61*).

272 In Hofbauer cells, the G2/M checkpoint signaling pathway, PI3K-AKT-mTOR signaling pathway,
273 and protein secretion were suppressed in both obesity groups, suggesting dysregulation of cell
274 proliferation, nutrient-sensing and tissue growth in maternal obesity (Fig. 4D). These changes might
275 represent an adaptive mechanism in Hofbauer cells to curb excessive cytokines and nutrient stress
276 in the placenta under obesity conditions. Notably, hypoxia, IL2-STAT5 signaling, inflammatory
277 response, and TNF-α signaling via NF-kβ were upregulated only in O-L, suggesting that
278 inflammatory and metabolic stress impaired placental homeostasis in O-L (Fig. 4D). Next, we
279 identified 30 genes regulated by maternal obesity (Fig. 4E). Most intriguingly, 14 genes were
280 altered differently in O-L or O-A (Fig. 4F). Among the genes upregulated only in O-L, *FKBP5*
281 encodes for a member of the immunophilin protein family that stabilizes glucocorticoids receptor
282 and promotes NFKβ-mediated inflammation in response to reactive oxidative species (*62*).
283 *NAMPT*, also known as Visfatin or PBEF, has a dual role as an enzyme and a cytokine regulating
284 glucose homeostasis (*63*). *SRGN* encodes a major secreted proteoglycan in macrophages and
285 promotes TNF-α secretion upon lipopolysaccharide stimulation (*64*). Of note, *ADAMTS2* was only
286 upregulated in O-A but not in O-L. *ADAMTS2* is a secreted metalloproteinase that processes
287 procollagen into collagen, a critical step for extracellular matrix stability. Its expression has been
288 implied as part of an anti-inflammatory response to contributing to tissue homeostasis (*65*), which
289 is consistent with increased inflammatory responses in O-L.

290 Another essential cell type in the villous core is the fibroblast. It is critical for villi architecture,
291 vascular development, immune regulation, and support of trophoblast functions. In fibroblasts, the
292 hallmark gene sets for KRAS signaling, PI3K-AKT mTOR signaling, adipogenesis and apoptosis,
293 were suppressed in both O-A and O-L, while TNF-α signaling via NFKβ was upregulated only in
294 O-L (Fig. 4G). We then identified 65 genes altered by maternal obesity and 18 genes by fetal growth
295 effects (Fig. 4H). Six genes that encode guanine nucleotide exchange factors to regulate GTPase
296 activity were decreased in both O-A and O-L (Fig 4I). These GTPase regulators control multiple
297 small GTPases that are involved in the feedback loop in PI3K activation (*66*). On the contrary,
298 *IRS2*, *PID1*, *SERPINE1, FOXO1, PDK4* were significantly upregulated in O-L while
299 downregulated in O-A (Fig. 4J). Notably, these genes are related to fatty acid response, insulin
300 receptor signaling and RTK signaling. FOXO1 could induce expression of *PDK4* (*67*), and it is also
301 a master regulator for TNF-α induced apoptosis and can inhibit the glucose metabolism (*68*).

302 *Cell-cell communication regulated by maternal and fetal growth effects in the placenta*

303 Our analyses have so far dissected the gene expression altered by maternal obesity and fetal growth
304 effects in major placental cell types. To further explore whether and how these cell types
305 communicate and coordinate transcriptional regulations in the placenta, we utilized the consensus
306 resources from LIANA+ (*69*) to examine the ligand-receptor (L-R) interactions among cell types.
307 To identify ligands expressed by each cell type that mediate signaling to other cell types, we first
308 constructed a weighted directional regulation network, mapping cell type-L to cell type-R (fig. S3).
309 To evaluate the biological relevance of these interactions, L-R interaction strength was calculated
310 with C-scores of gene pairs weighted by p-values. The altered genes in both O-A and O-L groups
311 were composed the L-R network regulated by maternal effects (Figure. 5A). While altered genes
312 differently between O-A and O-L composed the network related to fetal growth effects (Fig. 5B).
313 This analysis revealed VEC as the main cell type that sent the signals regulated by maternal effects
314 (Fig. 5A). And Hofbauer cells mainly sent signals associated with fetal growth effects (Fig. 5B).
315 Indeed, ligands from VEC, including *FN1*, *COL4A1* and *BMP6,* were among those highly ranked
316 out-degree genes in the network regulated by maternal effects (Fig. 5C). While ligands from
317 Hofbauer cells, including *SPP1*, *PDGFC* and *MAML2*, were highly ranked out-degree genes in the
318 network related to fetal growth effects. Similarly, we then analyzed in-degree scores across cell
319 types, representing the receiving of signaling based on receptor expression (Fig. 5D, E). We
320 identified STB-c as the primary signaling receiver, followed by CTBs, in network regulated by
321 maternal obesity (Fig. 5D). And fibroblasts were the main cell type receiving signaling related to
322 fetal growth from other cell types (Fig. 5E). By ranking in-degree scores of genes across cell types,
323 we identified that integrin complexes (*ITGA3-ITGB1*, *ITGAV-ITGB8*, *ITGA6-ITGB4*) were highly
324 ranked receptors expressed in STB-c regulated by maternal obesity, while *DSCAM* was the highest-
325 ranked receptor expressed in fibroblasts related to fetal growth (Fig. 5F).

326 Specifically, the main cell-cell communication regulated by maternal obesity was observed between
327 VEC and STB-c. The altered L-R pairs such as *VEGFC-FLT1*, *FN1-ITGAV*, *-ITGB3, and -FLT4*,
328 and *BMP6-BMPR2* (Fig. 5G) play a role in vascular formation, tissue structure, and cell fate
329 decisions. Moreover, top cell-cell communications related to fetal growth were observed between
330 Hofbauer and STB-c. The altered L-R pairs included *NAMPT-INSR* and *MAML2-NOTCH2.*
331 *NAMPT* functions as an intra- NAD biosynthetic enzyme and extracellular inflammation mediator,
332 and elevated extracellular NAMPT was reported in obesity (*70*). Additionally, *SPP1-ITGB1* and
333 *TIMP2-CD44* between Hofbauer and fibroblasts were altered differently in O-A or O-L (Fig. 5H).
334 *SPP1* encodes a multifunctional glycoprotein and the *Spp1*$^{+}$ macrophages emerged under obese
335 conditions in mice (*71*). *TIMP2* signaling was shown to stimulate fibroblast proliferation (*71*).

336 CTB was also a prominent signaling receiver at vasculo-syncytial membranes. Interestingly, we
337 found that most L-R interactions occurred between STB-c and CTB, involving growth-promoting
338 signaling pairs such as *CSHL1-GHR/PRLR*, *LAMA3-ITGB4*, *SEMA6A-PLXNA2* and
339 *ANXA1/TGFB1-EGFR,* among others (Fig. 5I). *CSHL1* encodes a human placental lactogen, that
340 can bind to the growth hormone receptor consisting of GHR and/or PRLR dimers. Additionally,
341 epidermal growth factor (EGF) is required for proper control of growth and differentiation of CTB
342 into STB (*72*) and altered EGFR expression has been associated with placental pathologies,
343 including intrauterine growth restriction (*73*). Interestingly, receptors for these growth-promoting
344 ligands were decreased in CTBs, suggesting active adaptation to maternal obesity.

Modeling the obese uterine milieu by co-culturing adipose spheroids and trophoblast organoids by a novel microfluidic system

Although it is well-established that maternal obesity affects placental function and offspring outcomes, the role of different maternal organs and tissue–tissue communication with the placenta remains unclear. Therefore, we investigated whether any observed transcriptional changes in the placenta could be attributed to communication between the adipose tissue and the placenta. To do so, we adopted a microfluidic co-culture system with medium flowing from primary adipose spheroids (ASs) to human term placenta-derived trophoblast organoids (TOs). The main component of the fluidic device contains interconnected tissue chambers, arranged in pairs, enabling parallel perfusion for triplicate experiments (*74*). To ensure gas permeability and conformal contact, a PDMS layer—never in direct contact with the culture media—was applied over the fluidic layer, and finally, an additional layer of PMMA was mounted on the top. It provided a stable chip-to-world connection and ensured sealed perfusion when inlet and outlet connectors are assembled (Fig. 6A). The medium was optimized for glucose, insulin and free fatty acids to simulate an obesity-like environment, consistent with its prior use for ASs culture (*75*). The first chamber pair of the microfluidic chip was designated for a medium control condition without ASs and in the second chamber pair, we placed ASs grown in the "obesity-like" conditions (*75, 76*) before seeded into the device for a 4.5-day co-culture. The ASs were established from white adipose tissue of female origin and cultured for a total of 17 days in "obesity-like" conditions before introduced in the microfluidic device. ASs displayed large lipid droplets stained by BODIPY, consistent with previous (*75*) (Fig. 6B). TOs exhibited a typical morphology with CTBs forming the outer layer shown by E-cadherin staining, and STBs embedded inside the inner layers shown by CGβ staining as shown previously in Matrigel embedded cultures (*77*) (Fig. 6B).

To examine how TOs were affected by secreted factor from "obesity-like" ASs, we performed bulk RNAseq of the TOs. Indeed, after the continuous exposure to obese ASs, the TO transcriptome was altered, with 188 differentially expressed genes (DEGs; 120 upregulated and 68 downregulated) when compared to medium control condition. Among the upregulated genes, *LEP*, *IGF2*, *PPARG* and *ASCL2* are related to placenta development, while *KISS1*, *HTRA4*, *ADAM12*, *PLAC4*, *INHA*, *HLA-G*, *FSTL3*, *ENG* are related to pre-eclampsia (Fig. 6C). On the contrary, metallothionein-encoding genes *MT1A, MT1E, MT1X,* and *MT2A* were significantly downregulated, suggesting impaired cellular response to ions such as zinc (Fig. 6C). Next, we compared 188 DEGs found in TOs with DEGs of all trophoblast cell types from our snRNA-seq analysis (Appendix Table S4). A total of 27 overlapping genes were identified, with 26 shared with STBs and one shared exclusively with CTB (Fig. 6D), which aligned with the cellular composition of TOs consisting predominantly of STB and a smaller population of CTBs. Importantly, many genes were highly expressed in TOs co-cultured with AS in "obesity-like" conditions (Fig. 6E). These included genes encoding placenta-specific secreted proteins (*46*), including *CGA*, *PSG3, PSG11*, *CSH2* and *TFPI2* (Fig. 6E). *LGALS14*, important for membrane integrity, was also upregulated (Fig. 6E). Interestingly, these 26 overlapping DEGs were all regulated in STB in O-A and O-L from the snRNA-seq analysis. The altered gene expression related with fetal growth effects, however, was not recapitulated by adipose tissue-derived signaling, and could potentially be ascribed to placental-fetal interactions.

To further confirm that, we investigated whether the identified fetal growth effects are linked to genetic loci, previously identified by genome-wide association studies (GWAS), associated with birth weight (*78*) and childhood BMI (*79*). We used MAGMA, a tool for generalized gene-set analysis of GWAS data, to analyze the statistical association between the aggregate genetic risk at

390 the gene-level (*80, 81*). To ensure reliable results, we excluded cell types from this analysis with
391 less than 10 DEGs. For remaining placental cell types, we did not find strong associations between
392 genes that were altered related to fetal growth effects at the transcription level and risk genes at the
393 genetic variation level (Fig. 6F). This suggests that transcriptional alterations identified as fetal-
394 growth effects might not be attributed to fetal genetic effects but placental-fetal interactions to
395 accommodate the fetal growth.
396
397 **Discussion**

398 Maternal obesity during pregnancy is associated with several adverse outcomes for both mothers
399 and offspring. A deeper deciphering of the molecular mechanisms underlying placental responses
400 is crucial for future interventions and therapeutic development. In this study, we examined
401 placentas of women with obesity who did not develop other pregnancy complications but delivered
402 either AGA or LGA infants (*28*). This could help minimize confounding factors and allow for a
403 clearer understanding of inherent placental alterations. Given that the human placenta is a highly
404 specialized organ with distinct cell types, including the multinucleated STB layer, we utilized
405 snRNA-seq to reveal cell-type-specific transcriptional responses to maternal obesity and fetal
406 growth. Notably, we were able to identify a set of transcriptional changes across placentas affected
407 by maternal obesity, regardless of fetal growth effects, highlighting these as maternal effects.
408 Moreover, we identified a distinct set of transcriptional changes that differed between O-A and O-
409 L, potentially related to different fetal growth effects. We further examined cell-cell communication
410 in mediating these maternal or fetal growth effects, highlighting key L-R pairs. Notably, VEC, STB,
411 Hofbauer cells and fibroblasts played prominent roles in such communications. These findings are
412 summarized in Figure 7.

413 Previous studies have shown that altered metabolites, hormones and cytokines - such as IL-6 and
414 TNF-α - in maternal obesity can be sensed by trophoblast cells, thereby influencing trophoblast
415 proliferation, nutrient uptake and transport (*82, 83*). Furthermore, activation of phospholipase A2
416 by TNF-α and leptin in human trophoblast cells has been proposed as a mechanism contributing to
417 excessive fetal fat accumulation and neonatal adiposity (*84*). In line with this, our findings reveal
418 that STB exhibit an enrichment of pathways related to elevated hypoxia and TNF-α signaling via
419 NF-kβ in maternal obesity. These responses were potentially driven by alterations in genes involved
420 in the cross-regulations of these pathways, such as *FOS*, *FOXO1*, and *SLC2A1*. *SLC2A1* is of
421 particular interest as it encodes GLUT1 to promote glucose uptake, suggesting that, similar to other
422 metabolic organs, there is an interplay between hypoxia, inflammation and excessive nutrient
423 transport specifically in the STB. Interestingly, we have recently demonstrated how mild
424 hyperglycemia can still induce placental hypoxia in mice, suggesting excessive hypoxia as a
425 common placental signature in maternal metabolic disorders (*85*).

426 Notably, in maternal obesity, CTBs downregulated genes involved in PI3K-Akt signaling
427 pathways, particularly those RTKs associated with the *GHR*, *PRLR*, and *CSF3R*. It is likely that the
428 altered expression of these receptors in CTBs is an active adaptation to the altered ligands expressed
429 in STB. When analyzing these L-R interactions between two cell types within placental villi, we
430 further found that mature STB-c altered the expression of growth-promoting ligands that could bind
431 to receptors in CTBs, which were generally downregulated, including growth factors receptors
432 binding to insulin-like growth factor, prolactin, and colony-stimulating factors (*86, 87*). Likely,
433 downregulation of these receptors in CTB followed by PI3K-Akt signaling pathways could dampen
434 the tissue growth signaling and serve as a potential link to maternal obesity.

435 Importantly, we further uncovered the molecular regulation related with the fetal growth in maternal
436 obesity. Notably, TNF-α signaling and inflammatory response were decreased in the Hofbauer cells
437 in O-A, whereas they were prominently increased in O-L, implying that LGA in maternal obesity
438 is strongly associated with inflammation. Aligning with this, *NAMPT* and *SLC1A3,* which play a
439 dual role in this inflammatory response and metabolism *(88),* were exclusively upregulated in O-L.
440 These genes likely facilitate the immune-metabolic modulation by Hofbauer cells related to fetal
441 overgrowth. Moreover, L-R network analysis revealed that Hofbauer cells sent the ligands
442 differently altered by fetal growth effects to other cell types in the villi. Hofbauer cells in O-L highly
443 expressed the ligand *SPP1,* and $SPP1^+$ macrophages have been reported to be in proximity to
444 hypoxic areas in tumors, to support tumor progression by promoting cell survival, angiogenesis,
445 and immunosuppression *(89)*. In addition, dysregulated Hofbauer polarization and immune
446 regulation can also restrict fetal growth (*90-92*). Therefore, Hofbauer cells may serve as a crucial
447 link in modulating fetal growth effects in response to hypoxic and inflammatory uterine
448 environment in maternal obesity.

449 Moreover, an increase in TNF-α signaling in fibroblasts was also observed exclusively in O-L. This
450 signaling may impair insulin action on fibroblasts by inhibiting the activation of IGF-1/insulin
451 hybrid receptors (*93*). In fibroblasts, the concurrent increase of TNF-α signaling and genes involved
452 in insulin receptor signaling, such as *IRS2,* suggests that these regulatory mechanisms may be
453 another contributor to fetal overgrowth. In line with this, we identified fibroblasts as the major
454 signaling receiver associated with fetal overgrowth, with the most expressed ligand being
455 macrophage-derived *SPP1*, which has been shown to activate myofibroblasts in fibrosis (*94*).
456 Fibroblasts and stromal cells in the term placenta have been understudied in prior research, our
457 analysis highlights their transcriptional responses to maternal obesity, particularly with fetal
458 overgrowth. Interestingly, TNF-α signaling was increased in STB of both obesity groups but only
459 increased in Hofbauer cells and fibroblasts in O-L. This may indicate that the STB response to
460 TNF-α is predominantly shaped by direct exposure to maternal circulating inflammatory signals,
461 whilst within the placental villi, these maternal signals need to be dampened to achieve appropriate
462 fetal growth. Regulatory mechanisms to protect the placental environment from excessive
463 inflammatory responses might be critical to proper fetal growth, while excessive inflammation
464 within villous niche likely related to fetal overgrowth. It would be valuable to further explore
465 whether targeting Hofbauer-specific inflammatory signaling pathways can mitigate fetal
466 overgrowth and thereby reduce the linked risk of cardiometabolic disorders in adulthood.

467 When investigating the intercellular communication network, we found that STB is the primary
468 'receiver' for the overall L-R pairs in maternal obesity regardless of fetal growth. Whether these
469 signals originate from maternal circulation or villous cells cannot be concluded from the snRNA-
470 seq data. Complement to this, we used a novel microfluidic system to co-culture TOs and ASs. This
471 confirmed that certain signals were likely of maternal origin, due to tissue-tissue communication.
472 Our microfluidic co-culture system displayed several advantages for studying the functional impact
473 of tissue communication. The unidirectional media flow from ASs to TOs simulated the effects of
474 potential metabolites and cytokines from the maternal circulation on the placenta. As DEGs in TOs
475 exhibited a greater overlap of altered genesto maternal obesity in STB, including *FLT1* and *PPARG,*
476 compared to other cell types, this further suggests the key role of STB regulation by the maternal
477 environment. Our co-culture system could not find any genes altered differently by fetal growth
478 effects in STBs, suggesting that factors other than the uterine milieu governs such fetal effects.
479 Interestingly, genes transcriptionally altered differently by fetal growth effects are not among those
480 genetic loci identified by GWAS of birthweight and childhood obesity. This further suggested the

importance of the placental-fetal interplay. Future investigations into the intricate dynamics of placental–fetal interactions will fundamentally reshape our understanding of this developmental processes. However, such experiments require innovative technological advances on embryo models. Importantly, our findings reveal promising molecular targets for further exploration.

In conclusion, our study demonstrates an intricated cell type-specific regulatory network within the placenta, driven by critical pathways such as hypoxia, nutrient transport, inflammation, and TNF-α signaling in maternal obesity and fetal overgrowth. Given the rising prevalence of global obesity, these mechanistic insights will deepen our understanding of placental interplay with fetal development. By precisely modulating these pathways, we can potentially mitigate pregnancy complications and lower the long-term risk of adverse health outcomes in offspring.

Materials and Methods

Experimental Design

The Institutional Ethics Committee for Research on Humans of the Faculty of Medicine, University of Chile (Protocol Nr. 033-2013, 201-201, 236–2020) reviewed and approved the protocol. At the time of recruitment, each participant received all information regarding the study, voluntarily enrolled and signed the informed consent. Women were recruited before delivery at the Maternity Service of the Hospital San Juan Dios, West Health Division, Santiago, Chile between 2014 and 2022. From the 328 placentas collected during this period, women with pregnancy complications such as hypertension, preeclampsia, thyroid disorders, GDM, preterm delivery, a fetus with malformations or chromosomal aberrations, and those with pregestational antecedents of diabetes, polycystic ovary syndrome, infertility, and assisted fertilization (IVF or ICSI) as well as those who declared to smoke, drink alcohol or take drugs during the pregnancy were excluded from this study. To the purpose of this study, women with normal pregestational weight (BMI between 18.50 -24.99 kg/m^2, n = 22) or pregestational obesity grade I (BMI between 30 – 35.7 kg/ m^2, n = 25) aged between 18 and 34 years old, that delivered from vaginal deliveries were further selected. Birth weight appropriate to gestational age (AGA) was defined as a birthweight more than 10th and below 90th percentile and birth weight large to gestational age (LGA) was defined as a birthweight above 90th percentile of the sex-specific and gestational age-specific reference mean(*6*). For single-nucleus analysis, placenta samples from control (normal-weight mothers and AGA babies, n=4), O-A (mothers with obesity and AGA babies, n=4), and O-L (mothers with obesity and LGA babies, n=4) were selected. And the maternal age, height, gestational age, and baby sex were not different between groups.

Sample collection

After delivery, placentas were collected as previously described (*28*) and snap frozen immediately in liquid nitrogen. Briefly, placentas from full-term pregnancies were collected immediately after delivery and processed within 30min. Each placenta was sectioned transversely using a sterile scalpel near the cord insertion site (approximately 5 cm) and villous part was used for snRNA-seq. The samples were then conserved in -80°C freezers until transport to Sweden when they were kept on dry ice and then store again in -80°C freezers. Newborn data such as sex, weight, height, and head circumference were recorded. Placental efficiency was calculated as the ratio of neonatal weight (g) to placental weight (g).

Nucleus isolation

525 Protocol for nucleus isolation was adapted from the protocol optimized for human placenta samples
526 by Ludivine Doridot and her team (Institut Cochin, France). Briefly, 30mg of frozen placenta was
527 chopped into small pieces on dry ice and added to douncer with cold NP-40 lysis buffer containing
528 RNase inhibitor. After 10min of incubation on ice, lysis buffer was diluted in wash medium (cold
529 PBS with 2% BSA and RNase inhibitor) and 10 strokes with the loose pestle were performed.
530 Samples were further filtered (100µm) and centrifuged at 600g, for 5 min at 4C. Pellet was
531 resuspended in cold wash medium, and then further filter (40µm) and centrifuged again. After
532 resuspension in nuclei resuspension buffer (1% BSA and RNase inhibitor solution in DPBS), the
533 pellet was filtered one last time (20µm).

534 The number of isolated nuclei was determined using trypan blue staining and automated cell counter
535 (Biorad, TC20) and quality of nuclei was assessed by visualization under microscope (EVOS XL
536 Core, ThermoFisher Scientific).

537 10x Genomics library preparation and sequencing

538 Suspension of good quality nuclei were processed as manufacturer's protocol for the Chromium
539 Single Cell 3' kit v3.1 (10X Genomics). Library preparation was performed to obtain between 1,000
540 and 10,000 nuclei per reaction. Libraries were then sequenced to obtained 90GB of data (paired
541 end, 150bp) per reaction on the Illumina NovaSeq 6000 at Novogene, UK.

542 snRNA-seq processing

543 Gene counts were obtained by aligning reads to the GRCh38 genome using Cell Ranger software
544 (10x Genomics). We used scanpy (*95*) to process and cluster the expression profiles and infer cell
545 identities of major cell classes. Cellbender (*96*) was used to remove background noise. In addition,
546 using Scrublet (*97*), cells that were labeled as doublets were removed.

547 For the UMAP visualization of individual major cell type classes, the analytical Pearson residue
548 was used to find the highly variable genes from individual batches. We selected the set of relevant
549 principal components based on elbow plots. High resolution cell clusters were identified using the
550 Leiden clustering algorithm. We annotated cell types using previously published marker genes and
551 single-cell RNA-sequencing data (*29*).

552 For the Pseudo-time analysis of trophoblast nuclei, Slingshot (*98*) was applied. Slingshot was
553 designed to identify a minimum spanning tree (MST). In this setting, pCTB was assigned as an
554 initial cell state and STB was classified as a terminal cell state.

555 We integrate the syncytiotrophoblast data generated in this study with the syncytiotrophoblast data
556 from the public human healthy term placenta snRNA-seq data (*99*) into the same embedding using
557 scANVI (*38*). We transferred their label onto our nuclei and compared the transferred labels with
558 our labels using the sihouette metric. The silhouette metric' values range from [−1, 1] with 1
559 indicates distinct labels, 0 indicates overlapping labels. Thus, the absolute value of the silhouette
560 width is used to measure how well labels are mixed.

561 We applied a Bayesian model in scCODA (*100*) for testing the compositional differences across
562 groups. pCTB population was selected as the reference cell type, which is assumed to be unchanged
563 in absolute abundance, and parameters inference was calculated via Hamiltonian Monte Carlo
564 (HMC) sampling.

565 Differential expression of obesity groups *vs* control

566 We performed differential expression analyses using a Wald test with a negative binomial
567 regression model using the formula "~ 1 + group + sex + log_number_of_genes" on raw counts.
568 Such analysis is deployed in R Seurat package (*101*). By default, in FindMarkers function in Seurat,
569 genes with more than one count in at least 1% of cells were considered. This rendered 6,000 to
570 7,000 genes to be analyzed. FDR was estimated with Benjamini-Hochberg method. The statistics
571 from this analysis were used as the input in the following method section.

572 For the gene set enrichment analysis, we ranked the genes in O-A vs. Control and O-L vs. Control
573 differential gene expression analysis respectively by fold changes. We then performed GSEA (*102*)
574 to get the normalized enrichment scores. Specifically, an enrichment score was calculated by
575 walking down the list of genes, increasing a running-sum statistic when a feature in each hallmark
576 gene set is encountered and decreasing it when it is not. The final score is the maximum deviation
577 from zero encountered in the random walk. Finally, a normalized score was obtained by computing
578 the z-score of the estimate compared to a null distribution obtained from N random permutations.
579 The p-values were adjusted by the BH method (*103*) to control the false discovery rate.

580 Gene Ontology enrichment analyses were performed using Enrichr (*55*). Specifically, Fisher's
581 exact test was used to test the overrepresentation of the gene sets of interest from this study in
582 known gene sets from MsigDB Hallmark database. The p-value from the test was adjusted with the
583 BH method.

584 Scoring the shared or different DEGs between comparisons

585 To measure the similarities or differences in differential gene expression between the two obese
586 groups and the normal weight group, we construct a score based on the fold changes of the genes
587 and the false discovery rates (FDRs) of the two comparisons:

588 $$Score = Magnitude \times Ratio$$

589 $$Magnitude = |E1 \times wFDR_{E1}| + |E2 \times wFDR_{E2}|$$

590 $$Ratio = \begin{cases} \dfrac{\max(E1, E2)}{|E1 - E2| + 1}, & E1 \times E2 > 0 \\ -\dfrac{|E1 - E2|}{\max(|E1|, |E2|) + 1}, & E1 \times E2 \leq 0 \end{cases}$$

591 $$wFDR = \begin{cases} 1, & FDR < 0.05 \\ \dfrac{log_{10}FDR}{log_{10}0.05}, & FDR \geq 0.05 \end{cases}$$

592 $E1 \coloneqq NES\ or\ log_2FC\ for\ O - A\ vs\ Control, C2 \coloneqq NES\ or\ log_2FC\ for\ O -$
593 $L\ vs\ Control$

594 A positive score indicates that the genes were both increased and decreased in the two comparisons.
595 The higher the score, the more similar and larger fold changes were. Conversely, a negative score
596 indicates that the gene was oppositely expressed in the two obese groups compared to the normal
597 weight group. This means that it was increased in one comparison group and decreased in the other.

598 The more negative the score, the more divergent and larger fold changes the gene had. In this
599 algorithm, genes with zero-fold changes were scored as zero.

600 To measure the significance of the scores of genes that were differentially expressed (score≠0), we
601 performed a permutation test. The fold changes and FDRs of all these genes in each comparison
602 were permuted 40,000 times if the number of genes with a score≠0 was over 200, otherwise, they
603 were permuted $(\text{number of the genes})^2$ times. The p-values were calculated to the observed
604 scores as the frequencies of the permutated scores > the observed score when the observed score is
605 positive or as frequencies of permuted scores < the observed score when the observed score is
606 negative. A one-sided p-value < 0.05 was used for significance.

607 Cell-cell communication (CCC) network analysis

608 Ligand–receptor interactions contrasts across cell type pairs were inferred using the consensus
609 ligand–receptor database from LIANA+ (*104*). The ligand-receptor edges were weighted by the
610 sum of C-scores for the corresponding genes obtained with the method stated in the preceding
611 section. This generated the cellA–cellB–ligand–receptor interaction tetramers weighted by the
612 similarity (C-scores) of the response in the two obesity groups vs control. The mean p-values for
613 the C-scores of the corresponding genes were assigned to the tetramers indicating significance of
614 the interaction as a response to maternal obesity.

615 From the weighted CCC network, the in-degree, out-degree, and betweenness centrality were
616 calculated. Betweenness centrality measures the extent to which a vertex lies on paths between
617 other vertices. Vertices with high betweenness may have considerable influence within a network
618 by virtue of their control over information passing between others. They are also the ones whose
619 removal from the network will most disrupt communications between other vertices because they
620 lie on the largest number of paths taken by messages.

621 Adipose spheroid establishment

622 Adipose spheroid (AS) obesity conditions were established as previously described. Briefly,
623 cryopreserved human primary stromal vascular fraction of white adipose tissue of female origin
624 were seeded in culture flasks with DMEM/F-12 Glutamax, 10% FBS and 1% penicillin-
625 streptomycin. After reaching the confluency of around 70%, cells were trypsinized and seeded into
626 ultra-low attachment 96-well plates (Corning) with 5,000 cells per well and centrifuged at 150g for
627 2 min. After 4 days, the culture medium was changed to serum-free differentiation medium
628 (William's E supplemented with 2mM L-Glutamine, 100 units/ml penicillin, 100µg/ml
629 streptomycin, 10µg/ml insulin, 10µg/ml transferrin, 6.7ng/ml sodium selenite and 100nM
630 dexamethasone; *differentiation cocktail*, 500µM 3-isobutyl-1-methylxanthine (IBMX), 10nM
631 hydrocortisone, 2nM 3,3',5-Triiodo-L-thyronine, 10µM rosiglitazone, 33µM biotin and 17µM
632 pantothenic acid, and *free fatty acids (FFAs)*, 160µM oleic acid; 160µM palmitic acid conjugated
633 to 10%BSA at a molar ratio of 1:5). After 48h, half of the medium was changed and subsequently
634 every 3-4 days for 17 days. After differentiation, the spheroids were transferred into the
635 maintenance media supplemented with FFAs for four days before the chip co-culture and the media
636 was exchanged every 2 days to phase out the differentiation growth factors.

637 Trophoblast organoid culture establishment

638 Villous trophoblast primary cells were isolated from human placental tissue as described previously
639 (*77*). Briefly, the isolated villi fragmented and washed intensely. Then, the tissue was digested with
640 0.2% trypsin (Alfa Aesar, J63993-09)/0.02% EDTA (Sigma-Aldrich, E9884) and 1 mg/mL

641 collagenase V (Sigma, C9263), and further disrupted by pipetting up and down with a serological
642 10mL pipette, around 10-15 times. The cellular digests were combined and washed with Advanced
643 DMEM/F12 medium (Life Technologies 12634-010), and cells were counted with a automatic cell
644 counter (TC20 BioRad). After, the cells were pelleted and resuspended in pre-thawed Matrigel
645 (Corning 35623). The volume of Matrigel is dependent on cell counting and on pellet size; in
646 general, at least 10x of cell pellet volume should be used. 20µL domes of Matrigel/cells were seeded
647 in a 48-well culture plate and placed in an incubator at 37°C with 5% CO_2 for 3 minutes, then the
648 plate was turned upside down so cells distribute evenly within the Matrigel domes. The domes were
649 incubated for a total of 15 minutes before supplemented with 250µL of trophoblast organoid
650 maintenance medium, composed with: Advanced DMEM/ F12 (Life Technologies, 12634-010); 1x
651 B27 (Life Technologies, 17504-044); 1x N2 (Life Technologies, 17502-048); 10% FBS (Cytiva
652 HyClone, SH30070.03); 2mM L-glutamine (Life Technologies, 35050-061); 100µg/mL Primocin
653 (InvivoGen, antpm-1); 1,25mM NAC (SigmaAldrich, A9165), 500nM A83-01 (Tocris, 2939);
654 1,5µM CHIR99021 (Tocris, 4423); 50ng/mL hEGF (Gibco, PHG0314); 80g/mL human R-
655 spondin1 (R&D systems, 4645-RS-100); 100ng/mL hFGF2 (Peprotech, 100-18C); 50ng/mL hHGF
656 (Peprotech, 100-39); 10mM nicotinamide (Sigma-Aldrich, N0636-100G); 5µM Y-27632 (Sigma,
657 Y0503-1MG); 2.5µM prostaglandin E2 (PGE2, R&D systems, 22- 961-0).Medium was replaced
658 every 2-3 days. hCG was measured to ensure proliferation of trophoblast cells using professional
659 pregnancy test strips (Gravidetstest GI29100, Medistore). Small trophoblast organoids became
660 noticeable and positive hCG tests were obtained around 10-15 days after establishment.

661 Maintenance and recovery of trophoblast organoids

662 Passages were performed every 5-7 days, as previously described by (*77*). Each Matrigel dome was
663 disintegrated by pipetting the medium up and down and by scraping. Organoid suspension was
664 washed and digested in pre-warmed StemPro Accutase (Gibco, A11105-01) with Y-27632 (Sigma,
665 Y0503-1MG) for 10 minutes at 37°C. After carefully removing the supernatant, 200µL of
666 Advanced DMEM/ F12 (Life Technologies, 12634-010) was added before performing mechanical
667 dissociation by at least 200 ups and downs, using an automatic pipette. Cell suspension was washed
668 and resuspended in cold Matrigel and plated into 20 µL domes with desired cell density. 250µL of
669 trophoblast organoid medium was added, after 15 minutes of incubation at 37°C with 5% CO_2.

670 After 7 days of culture, TOs were removed from Matrigel. For that, 250µL of Cell Recovery
671 Solution (Corning 354253) was added to each well. The plate was incubated on ice for 45 minutes.
672 The Matrigel domes were dissociated by gently pipetting up and down, the organoid/cell recovery
673 solution was collected and centrifuged. After removing the supernatant, the organoid pellet was
674 washed and resuspended in cold pre-thawed Matrigel. Tubes were kept on ice until the assembly of
675 the microfluidic co-culture.

676 Co-culture of trophoblast organoids with adipose spheroids on a microfluidic device

677 To co-culture obese AS with TOs, we used multilayered microfluidic devices made of off-
678 stoichiometric thiol–ene–epoxy (OSTE+), poly(methyl methacrylate) (PMMA) and
679 polydimethylsiloxane (PDMS). The OSTE+ parts, which hold the tissue chambers (D = 6 mm) and
680 microfluidic channels (W= 1000 µm, H = 500 µm), were produced from OSTEMER-322 (Mercene
681 labs, Sweden), as previously described (*74*). The PDMS layer was cast and the PMMA layer was
682 cut using a micromilling machine (Minitech Machinery Corp., USA). The AS were grown and
683 differentiated for 17 days and washed in maintenance media before the chip culture. Between 20 to
684 30 AS were loaded in the first chambers of the co-culture chips and 17 µL domes of TOs (grown
685 for seven days after splitting) were seeded in Matrigel in the second chambers of all devices. The

686 control chips were only seeded with TOs. To mimic an obese environment, obesogenic media
687 (previously described) was perfused at a constant flow rate of 5µL/minute using an NE-1600
688 SyringeSIX Programmable Multichannel Syring Pump (New Era Pump Systems Inc.). After 4 days,
689 TB-Org were collected for RNA-extraction.

690 RNA extraction and sequencing of trophoblast organoids

691 TOs for RNAseq analysis were recovered from Matrigel using Cell Recovery Solution (Corning,
692 354253), as described previously. 500µL of cold TRI reagent (Sigma-Aldrich) was added and
693 incubated on ice for 5 minutes. Then 100µL of chloroform was added, vortex mixed and
694 centrifuged. Around 200µL of supernatant was recovered and the same volume of isopropanol was
695 then added. The mixture was further mixed and loaded on Minicolumn (ReliaPrep RNA Miniprep,
696 Promega). The next steps were performed following manufacturer instructions and included DNase
697 treatment.

698 Prime-seq protocol was used to prepare RNA sequencing libraries as previously described (*105*).
699 Briefly, samples with 10ng/µL of extracted RNA were used for reverse transcription and pre-
700 amplification. The cDNA was quantified using the PicoGreen dsDNA Assay Kit (ThermoFisher
701 Scientific) and qualified using the Bioanalyzer High Sensitivity DNA chip (Agilent), before
702 subsequent library construction using the NEBNext Ultra II FS Kit (New England Biolabs). Then
703 the libraries were sequenced on Illumina NovaSeq 6000 at Novogene, UK at an average depth of
704 20 million reads per sample.

705 Downstream analysis of trophoblast organoid RNA sequencing

706 Quality of the raw data was checked using FastQC (version 0.11.9), trimmed of poly(A) tails using
707 Cutadapt (version 4.1), before filtering using the zUMIs pipeline (version 2.9.7) (*106*). The filtered
708 data was then mapped to the human genome using STAR (version 2.7.10a) (*107*), and reads were
709 counted using RSubread (version 2.12.0) (*108*). Lowly expressed genes (count sum <50 for all
710 samples) were filtered out before differential analysis. Differential expression analysis on RNA
711 sequencing data was done using the DESeq2 package (version 1.36.0) (*109*). Differentially
712 expressed genes (DEGs) were defined as adjusted p-value<0.05 and fold-change>2 or <-2.

713 Statistical Analysis

714 Variables (maternal age, height and BMI, birthweight, placental weight and efficiency) were
715 analyzed using GraphPad Prism 9.4.1 for Windows (GraphPad Software, San Diego, California
716 USA, www.graphpad.com). For cohort comparisons, t test with Welch's correction were applied.
717 For snRNA-seq sample data, Kruskal-Wallis test followed by two stage linear step procedure of
718 Benjamini, Krieger and Yekutieli for adjustment were performed. For all comparisons, a variable
719 was considered as significantly different between group for p after correction < 0.05. In the text,
720 data are represented as mean ± SEM.
721

Acknowledgments
This work is supported by the Swedish Medical Research Council: project nos. 2018-02557(Q.D.), 2020-00253(Q.D.) and 2022-00550 (E.S.-V.), 2021-02801 (V.M.L.), 2023-03015 (V.M.L.) and 2024-03401 (V.M.L.); the Knut and Alice Wallenberg Foundation: 2019.0211 (Q.D.) and VC-2021-0026 (V.M.L.); Karolinska Instiutet faculty funded position (Q.D.); Diabetes foundation: DIA2022-733 (Q.D.); Barndiabetes fonden (Q.D.); Distinguished Investigator Grant – Endocrinology and Metabolism, Novo Nordisk Foundation: NNF22OC0072904 (E.S.-V.); the Diabetes Foundation: DIA2021-633 (E.S.-V.); the Karolinska Institutet-China scholarship council program (H.J.); the Robert Bosch Foundation (V.M.L.), as well as the Innovative Medicines Initiative 2 Joint Undertaking (JU) under grant agreement No. 875510 (V.M.L.). The mapping of the sequencing data and ambient removal were performed using resources provided by the National Academic Infrastructure for Supercomputing in Sweden (NAISS), partially funded by the Swedish Research Council through grant agreement no. 2022-06725.

Author contributions
H.J contributed to the design of the work, analysis, and interpretation of data, the formulation of the C-score used in this work, and have drafted the work; E.D contributed to the design of the work, and the acquisition of the data; D.P contributed to the acquisition of the trophoblast organoids data and has revised the work; N.T contributed to the acquisition of the adipose spheroids and microfluidic co-culture system; R.Z.S fabricated and characterized the microfluidic devices; M.O contributed the acquisition of the placental tissues; P.R.J contributed to the acquisition of the trophoblast organoids and has revised the work; A.Z contributed to revise the work; C.L contributed to the library construction the placental tissues; M.A.M contributed to the acquisition of the placental samples; E.S-V contributed to the acquisition of the samples and revise the work; V.M.L contributed to microfluidic co-culture system and revise the work; Q.D conceptualized and designed the work, interpretation of the data, drafted the work. All authors contributed to revising the manuscript.

Disclosure and competing interests statement
V.M.L. is co-founder, CEO and shareholder of HepaPredict AB, as well as co-founder and shareholder of Shanghai Hepo Biotechnology Ltd. The other authors declare no competing interests.

Data and materials availability: Raw snRNA sequencing data from the placenta tissues and Raw RNA sequencing data from trophoblast organoids were deposited in EGAS50000000834. The explanation and script for C-score calculation and is available at https://github.com/DengLab-KI/cscore. The notebooks to reproduce the presented results is available at https://github.com/DengLab-KI/obesity_paper. Source data for reproducing the figures are deposited at Zenodo https://doi.org/10.5281/zenodo.14549513. Data on birth weight has been contributed by the EGG Consortium using the UK Biobank Resource and has been downloaded from www.egg-consortium.org. Data on childhood body mass index have been contributed by the EGG Consortium and have been downloaded from www.egg-consortium.org.

Figures

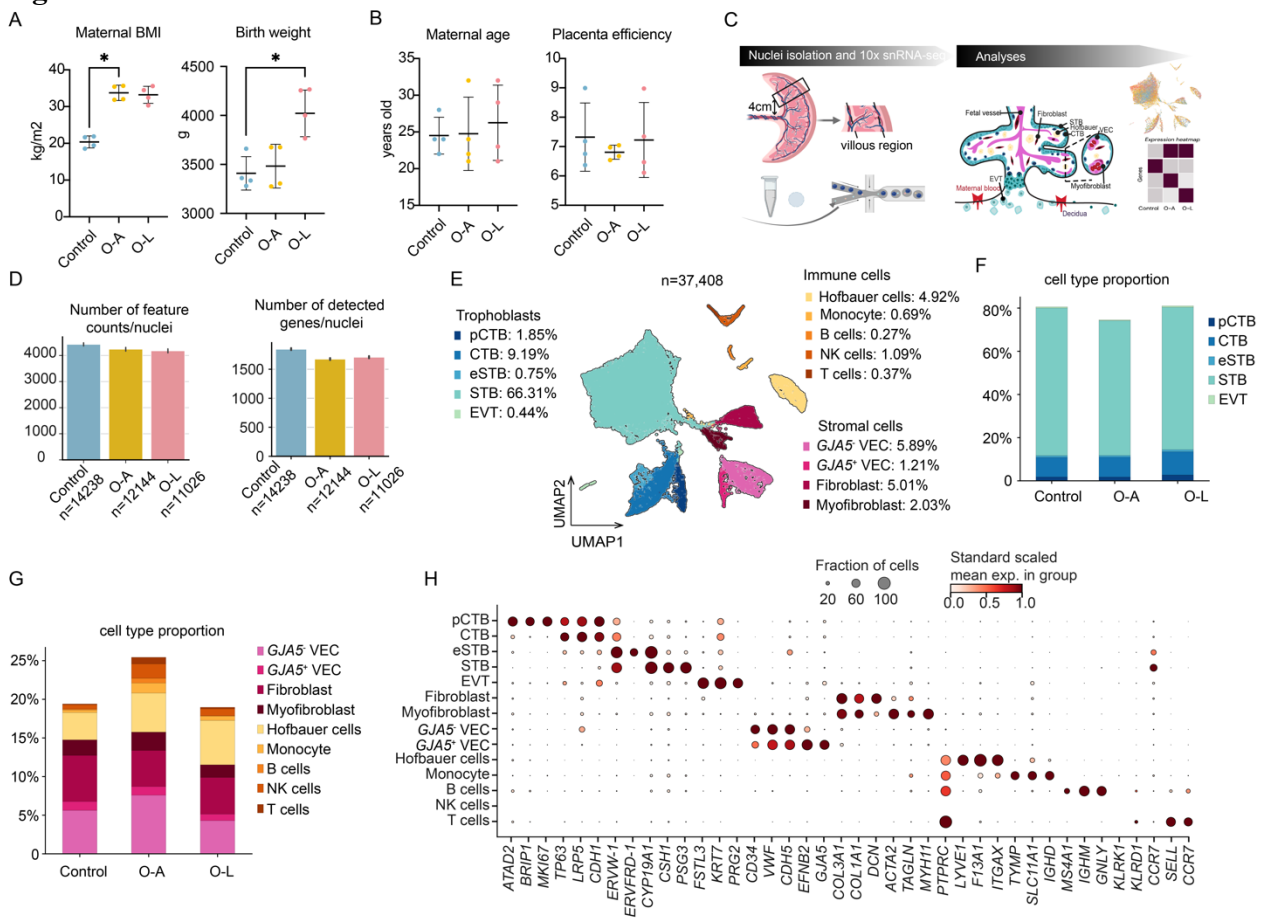

Fig. 1: snRNA-seq of human placentas from normal-weight mothers and mothers with obesity stratified by fetal birthweight. **(A)** Maternal BMI (body mass index), and birthweight of samples for snRNA-seq from each group. **(B)** Maternal age, and placental efficiency of samples for snRNA-seq from each group. **(C)** Experimental procedures. **(D)** Number of feature counts per nuclei and number of detected genes per nuclei. **(E)** Two-dimensional UMAP (Uniform manifold approximation and projection) of 37,408 nuclei profiles (dots) from all donors (n=12), colored by cell type. **(F)** Stacked barplot showing trophoblast cell proportion in each group. **(G)** Stacked barplot showing the proportion of non-trophoblast cell types i n each group. **(H)** Mean expression (dot color, gene standard scaled across all cells of a type) and fraction of expressing nuclei (dot size) of marker genes for each of the 14 major cell types. Controls: normal-weight women (n=4); O-A: Mothers with obesity with appropriate-for-gestational-age baby (birthweight within the 25th and 90th percentile of WHO growth curves); O-L: Mothers with obesity with large-for-gestational-age baby (birthweight >90th percentile of WHO growth curves); CTB: cytotrophoblasts; VEC: vascular endothelial cells; EVT: extravillous trophoblasts; pCTB: proliferative CTB; STB: syncytiotrophoblasts; eSTB: early syncytiotrophoblasts.

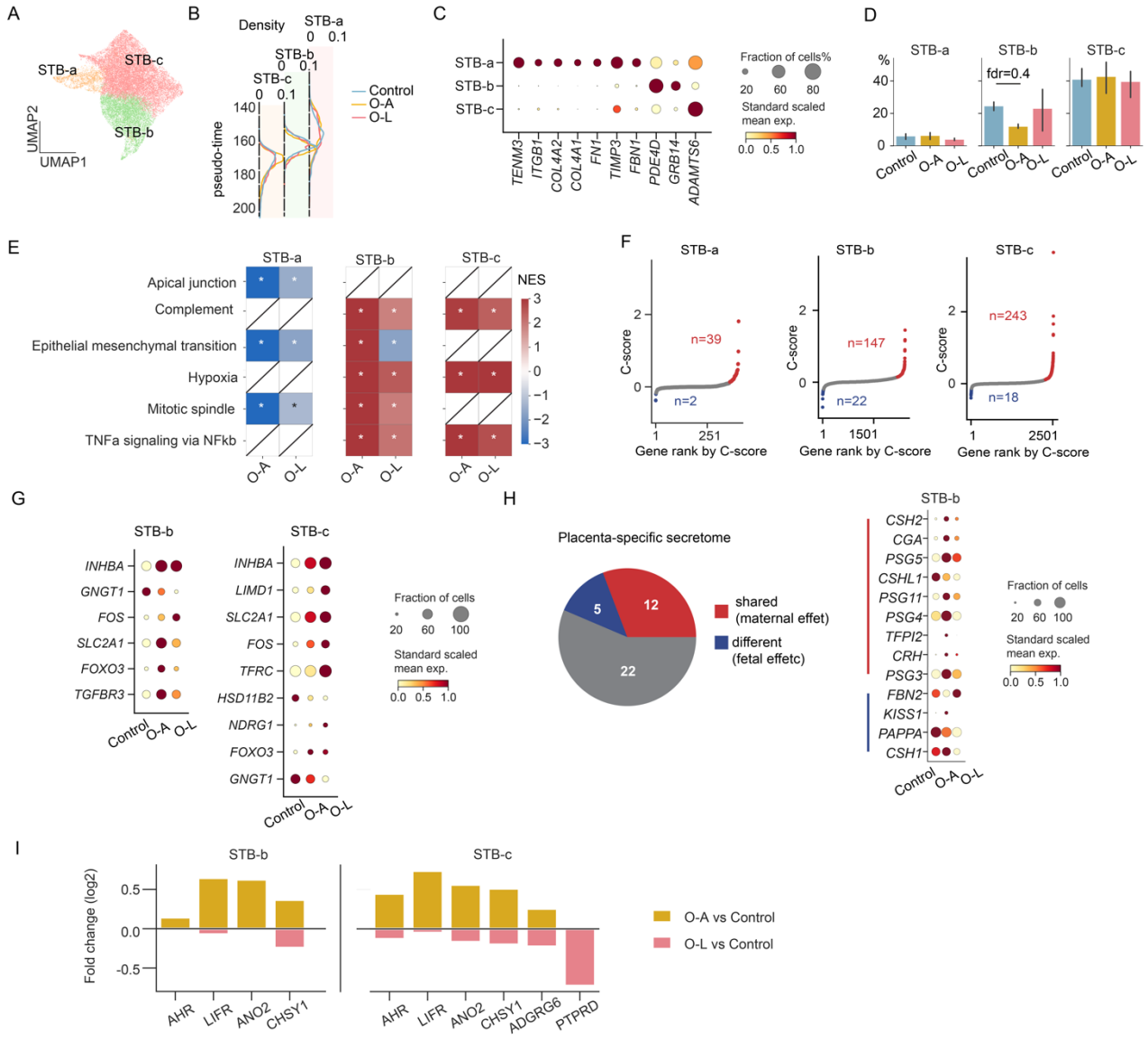

Fig. 2: Maternal obesity changed the expressionof hypoxia-, inflammation-nutrient transport-related pathway in STB nuclei. (A) UMAP representation of STB colored by STB states. **(B)** Pseudotime value visualization across trophoblast cell types and states. Density plot of pseudotime value colored by each group. **(C)** Dotplot of genes specifically expressed in STB-a, -b or -c state. Dot color indicates the standard-scaled mean expression level of the gene. **(D)** Proportion of STB states across groups. Bar height represents the mean and the error bar represents 50% interval. Data were compared by a Bayesian model. **(E)** Gene set enrichment analysis (GSEA) with the enrichment score of hallmark gene sets for O-A *vs* Control and O-L *vs* Control. NES: normalized enrichment score. *adjusted p-value < 0.05. **(F)** Scatterplots of genes ordered by C-scores in STB. **(G)** Dotplots showing the expression of the shared DEGs in O-A and O-L involved in hypoxia pathway. **(H)** The proportion of shared or different DEGs in O-A and O-L among the placenta-specific secretome reported in human protein atlas (*46*) (left). Dotplot showing the expression of the genes in STB-b that encode placenta-specific secreted proteins. **(I)** Barplots showing the fold changes of DEGs related to fetal growth effects (different in O-A and O-L) encoding for receptors, channels or molecular sensors.

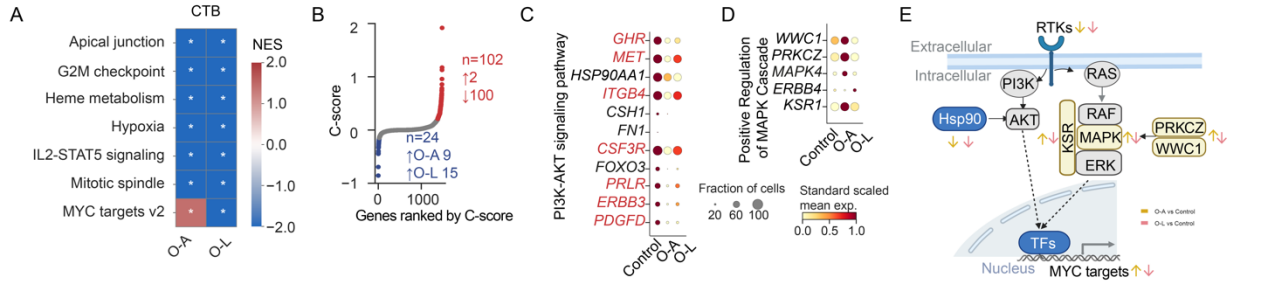

Fig. 3: Gene expression changesin PI3K-Akt pathway and MAPK cascade in CTBs from mothers with obesity with or without fetal overgrowth. (A) Gene set enrichment analysis (GSEA) with the enrichment score of hallmark gene sets for O-A *vs* Control and O-L *vs* Control. NES: normalized enrichment score. *indicates adjusted p-value < 0.05. **(B)** Scatterplots of genes ordered by C-scores in CTB. **(C)** Dotplots showing the expression of the genes involved in PI3K-Akt signaling pathway, and **(D)** positive regulation of MAPK cascade. **(E)** Summary of genes involved in the pathways downstream the receptor tyrosin kinase (RTK) signaling. The PI3K-Akt signaling was reduced in CTBs from both obesity groups, while the MAPK signaling was upregulated in O-A.

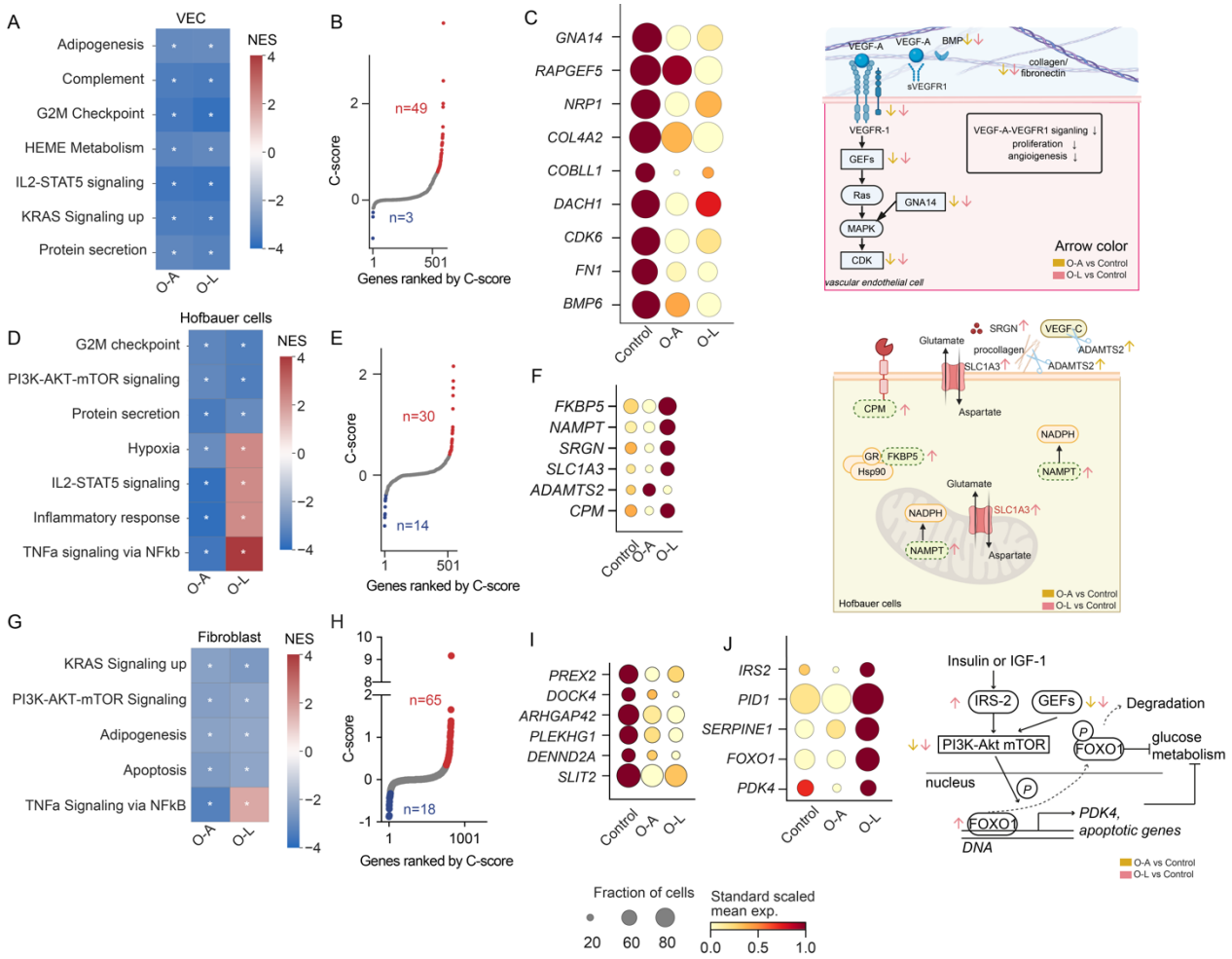

Fig. 4: Gene expression changes in vascular endothelial cells, Hofbauer cells and fibroblasts from placentas of mothers with obesity with or without fetal overgrowth. (A) Gene set enrichment analysis (GSEA) in vascular endothelial cells (VEC), with the enrichment score of hallmark gene sets for O-A *vs* Control and O-L *vs* Control. **(B)** Scatterplots of genes ordered by C-scores in VEC. **(C)** Dotplot showing expression of genes relevant to FLT1 (VEGFR1) (left). Summary of genes involved in VEGFR1 signaling (right). **(D)** GSEA in Hofbauer cells, with the enrichment score of hallmark gene sets for O-A *vs* Control and O-L *vs* Control. **(E)** Scatterplots of genes ordered by C-scores in Hofbauer cells. **(F)** Dotplot showing expression of genes involved in inflammatory response in Hofbauer cells (left). Summary of these genes in cellular context (right). **(G)** GSEA in fibroblast cells, with the enrichment score of hallmark gene sets for O-A *vs* Control and O-L *vs* Control. **(H)** Scatterplots of genes ordered by C-scores in fibroblasts. (**I**) Dotplot showing expression of genes related to GTPase activity that were changed in maternal obesity, and **(J)** the genes involved in PI3K-Akt pathway and guanine nucleotide exchange factors that were changed according to fetal growth effects. Summary of these genes within the PI3K-Akt-mTOR pathway (right). For **(A)**, **(D)**, **(G)**, NES: normalized enrichment score. *adjusted p-value < 0.05. For (**C**), (**F**), (**I**), the dot size is proportional to the fraction of cells that express the gene, and the color indicating the expression levels standard-scaled between 0 and 1.

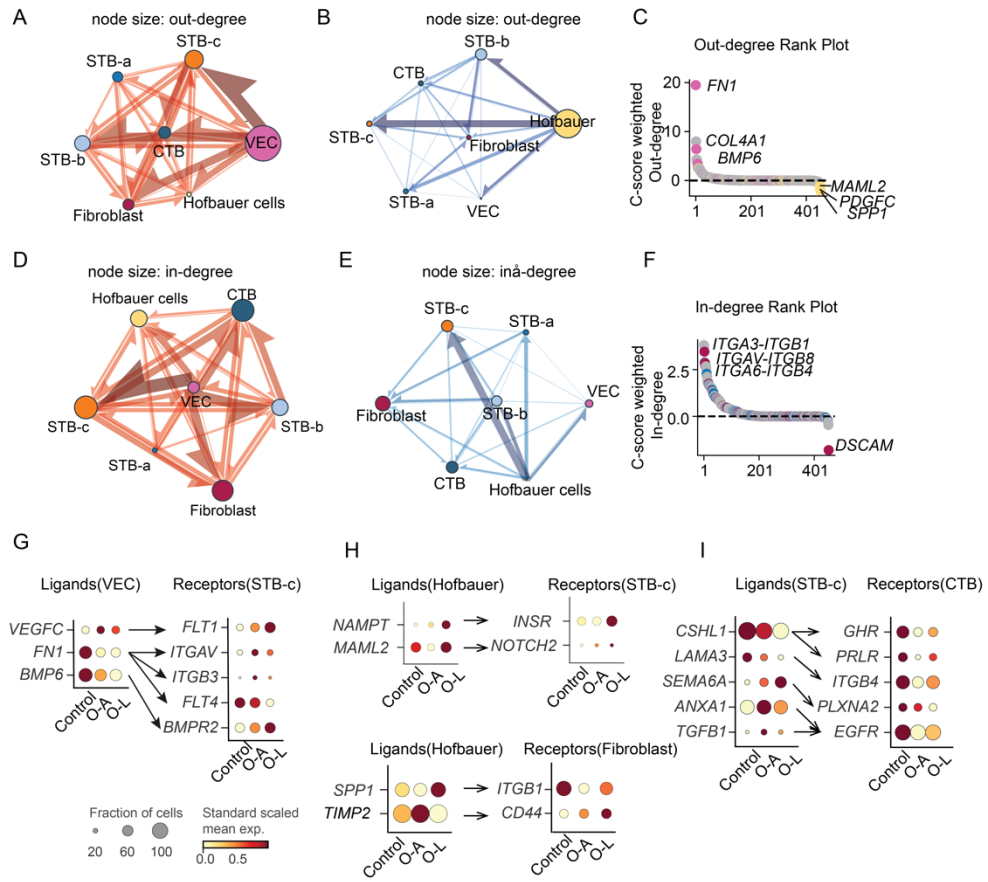

Fig. 5: Dysregulated cell-cell communication networks of mothers with obesity, with or without fetal overgrowth. (A) Connectome ring plots for cell-cell communication built from differentially expressed ligand-receptor pairs shared in maternal obesity groups and (**B**) differently according to fetal growth effects. Different colors represent different cell types, node size indicating out-degree, and edge direction goes from the sender cell type to the receiver cell type. **(C)** Out-

degree analysis indicating the major or sender cells of ligands regulated commonly in maternal obesity or differently according to fetal growth effects. Pink dots represent the vascular endothelial cells, and the yellow dots represent the Hofbauer cells. **(D)** Connectome ring plots built from ligands regulated in maternal obesity and (**E**) differently according to fetal growth effects among major cell types in placental villi from mothers with obesity. Different colors represent different cell types, node size indicating in-degree, and edge direction goes from the sender cell type to the receiver cell type. **(F)** In-degree analysis indicating the major receiver cells with receptors. Red dots represent fibroblasts, and blue dots represent STB-c. **(G)** Dot plot showing the expression of ligands from the VEC)and receptors from STB-c. **(H)** Dot plot showing the expression of ligands from Hofbauer cells and receptors from fibroblasts and STB-c. **(I)** Dot plot showing the expression of the ligands from STB-c and the receptors from CTB.

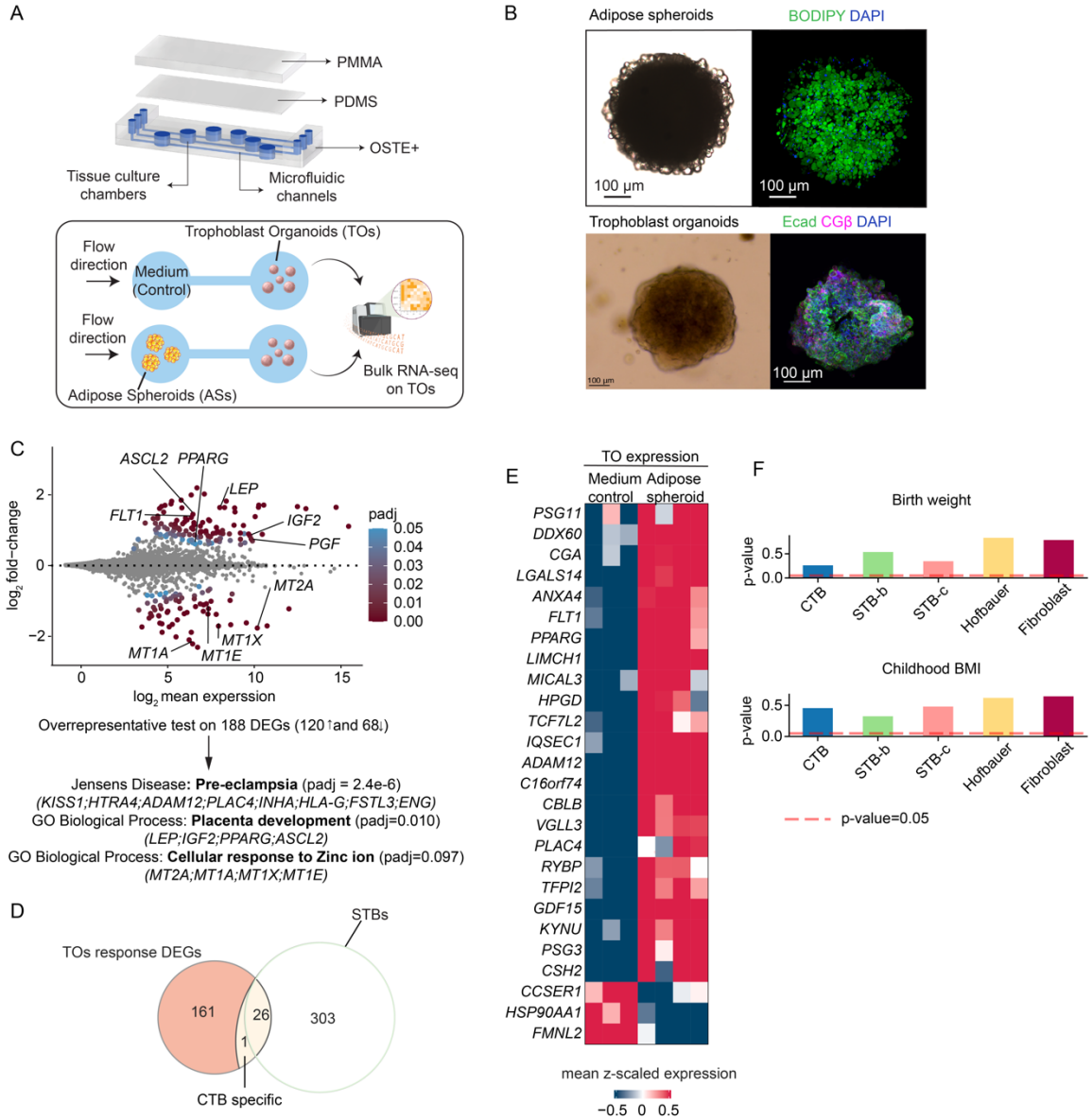

Fig. 6: Trophoblast organoids co-cultured with adipose spheroids recapitulated the transcriptional changes observed in STB of mothers with obesity. (A) Design of the microfluid device and co-culture experiment of Trophoblast Organoids (TOs) and adipose spheroids (ASs). **(B)** Representative images of ASs (up; bright-field image and confocal image stained with BODIPY

850 and DAPI to highlight neutral lipids and nuclei, respectively) and TOs (bottom; bright-field image
851 and confocal image stained with E-cadherin, CGβ and DAPI to highlight CTBs, STB and nuclei,
852 respectively). Images were captured with 10x magnification. **(C)** MA plot of gene expression in
853 TOs co-cultured with ASs compared with TOs cultured without ASs. **(D)** Venn diagram showing
854 the overlap of the differentially expressed genes in the microfluidic co-culture experiment and
855 trophoblast in maternal obesity groups. **(E)** Expression heatmap for the 26 overlapping genes in
856 (D). (**F**) Enrichment between cell type–specific differentially expressed genes related to fetal
857 growth effects and genomic variants implicated by GWAS for birth weight and childhood BMI
858 computed with MAGMA (*80, 81*).

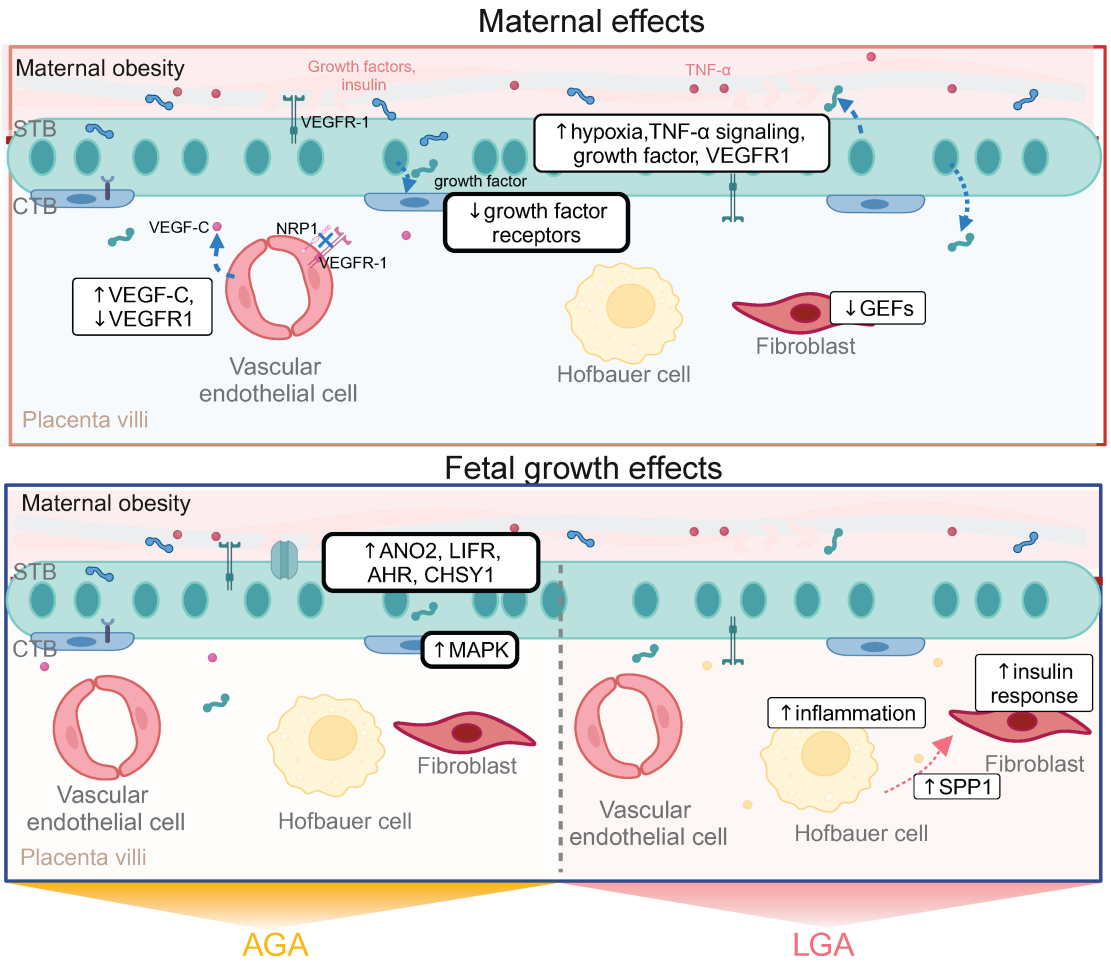

859

860 **Fig. 7:** Schematic summary showing that gene expression changes in maternal obesity and different
861 gene expression changes according to fetal growth effects, highlighting the genes involved in each
862 cell types.

863 **References**

864 1. N. C. D. R. F. Collaboration, Worldwide trends in underweight and obesity from 1990 to
865 2022: a pooled analysis of 3663 population-representative studies with 222 million
866 children, adolescents, and adults. *Lancet* **403**, 1027-1050 (2024).
867 2. P. M. Catalano, K. Shankar, Obesity and pregnancy: mechanisms of short term and long
868 term adverse consequences for mother and child. *BMJ* **356**, j1 (2017).
869 3. Obesity in Pregnancy: ACOG Practice Bulletin, Number 230. *Obstet Gynecol* **137**, e128-
870 e144 (2021).
871 4. C. X. W. Zhang, A. A. Candia, A. N. Sferruzzi-Perri, Placental inflammation, oxidative
872 stress, and fetal outcomes in maternal obesity. *Trends Endocrinol Metab* **35**, 638-647
873 (2024).
874 5. K. M. Godfrey *et al.*, Influence of maternal obesity on the long-term health of offspring.
875 *Lancet Diabetes Endocrinol* **5**, 53-64 (2017).
876 6. T. Kiserud *et al.*, The World Health Organization Fetal Growth Charts: A Multinational
877 Longitudinal Study of Ultrasound Biometric Measurements and Estimated Fetal Weight.
878 *PLoS Med* **14**, e1002220 (2017).
879 7. N. J. Sebire *et al.*, Maternal obesity and pregnancy outcome: a study of 287,213
880 pregnancies in London. *Int J Obes Relat Metab Disord* **25**, 1175-1182 (2001).
881 8. Y. Liu, W. Dai, X. Dai, Z. Li, Prepregnancy body mass index and gestational weight gain
882 with the outcome of pregnancy: a 13-year study of 292,568 cases in China. *Arch Gynecol*
883 *Obstet* **286**, 905-911 (2012).
884 9. P. Kalk *et al.*, Impact of maternal body mass index on neonatal outcome. *Eur J Med Res*
885 **14**, 216-222 (2009).
886 10. B. S. Richardson, S. Ruttinger, H. K. Brown, T. R. H. Regnault, B. de Vrijer, Maternal
887 body mass index impacts fetal-placental size at birth and umbilical cord oxygen values
888 with implications for regulatory mechanisms. *Early Hum Dev* **112**, 42-47 (2017).
889 11. S. Johansson *et al.*, Maternal overweight and obesity in early pregnancy and risk of infant
890 mortality: a population based cohort study in Sweden. *BMJ* **349**, g6572 (2014).
891 12. N. Heslehurst *et al.*, The association between maternal body mass index and child obesity:
892 A systematic review and meta-analysis. *Plos Medicine* **16**, (2019).
893 13. D. Lu *et al.*, Birth Weight, Gestational Age, and Risk of Cardiovascular Disease in Early
894 Adulthood: Influence of Familial Factors. *Am J Epidemiol* **192**, 866-877 (2023).
895 14. S. Santos *et al.*, Impact of maternal body mass index and gestational weight gain on
896 pregnancy complications: an individual participant data meta-analysis of European, North
897 American and Australian cohorts. *BJOG* **126**, 984-995 (2019).
898 15. J. M. Petersen *et al.*, Weight gain patterns among pregnancies with obesity and small- and
899 large-for-gestational-age births. *Obesity (Silver Spring)* **31**, 1133-1145 (2023).
900 16. L. Poston *et al.*, Effect of a behavioural intervention in obese pregnant women (the
901 UPBEAT study): a multicentre, randomised controlled trial. *Lancet Diabetes Endocrinol*
902 **3**, 767-777 (2015).
903 17. C. Chiswick *et al.*, Effect of metformin on maternal and fetal outcomes in obese pregnant
904 women (EMPOWaR): a randomised, double-blind, placebo-controlled trial. *Lancet*
905 *Diabetes Endocrinol* **3**, 778-786 (2015).
906 18. N. M. Gude, C. T. Roberts, B. Kalionis, R. G. King, Growth and function of the normal
907 human placenta. *Thromb Res* **114**, 397-407 (2004).
908 19. M. A. Costa, The endocrine function of human placenta: an overview. *Reprod Biomed*
909 *Online* **32**, 14-43 (2016).
910 20. S. Hauguel-de Mouzon, M. Guerre-Millo, The placenta cytokine network and
911 inflammatory signals. *Placenta* **27**, 794-798 (2006).
912 21. N. Jansson *et al.*, Activation of placental mTOR signaling and amino acid transporters in

913 obese women giving birth to large babies. *J Clin Endocrinol Metab* **98**, 105-113 (2013).
914 22. D. Newbern, M. Freemark, Placental hormones and the control of maternal metabolism
915 and fetal growth. *Curr Opin Endocrinol Diabetes Obes* **18**, 409-416 (2011).
916 23. J. Saben *et al.*, Maternal obesity is associated with a lipotoxic placental environment.
917 *Placenta* **35**, 171-177 (2014).
918 24. D. L. Armstrong *et al.*, The core transcriptome of mammalian placentas and the
919 divergence of expression with placental shape. *Placenta* **57**, 71-78 (2017).
920 25. S. Gong *et al.*, The RNA landscape of the human placenta in health and disease. *Nat*
921 *Commun* **12**, 2639 (2021).
922 26. S. Buckberry *et al.*, Placental transcriptome co-expression analysis reveals conserved
923 regulatory programs across gestation. *Bmc Genomics* **18**, 10 (2017).
924 27. S. Gong *et al.*, The human placenta exhibits a unique transcriptomic void. *Cell Rep* **42**,
925 112800 (2023).
926 28. M. Ortiz *et al.*, Association between maternal obesity, essential fatty acids and biomarkers
927 of fetal liver function. *Prostag Leukotr Ess* **190**, (2023).
928 29. E. Derisoud, H. Jiang, A. Zhao, P. Chavatte-Palmer, Q. Deng, Revealing the molecular
929 landscape of human placenta: a systematic review and meta-analysis of single-cell RNA
930 sequencing studies. *Hum Reprod Update* **30**, 410-441 (2024).
931 30. A. A. Adane, G. D. Mishra, L. R. Tooth, Diabetes in Pregnancy and Childhood Cognitive
932 Development: A Systematic Review. *Pediatrics* **137**, (2016).
933 31. S. A. El-Tarhouny, S. M. Almasry, A. K. Elfayomy, H. Baghdadi, F. A. Habib, Placental
934 growth factor and soluble Fms-like tyrosine kinase 1 in diabetic pregnancy: A possible
935 relation to distal villous immaturity. *Histol Histopathol* **29**, 259-272 (2014).
936 32. O. Nonn *et al.*, Disturbed trophoblast transition links preeclampsia progression from
937 placenta to the maternal syndrome. *bioRxiv*, 2022.2010.2010.511539 (2022).
938 33. P. Gerbaud, K. Tasken, G. Pidoux, Spatiotemporal regulation of cAMP signaling controls
939 the human trophoblast fusion. *Front Pharmacol* **6**, 202 (2015).
940 34. S. A. Cain, E. J. Mularczyk, M. Singh, T. Massam-Wu, C. M. Kielty, ADAMTS-10 and -6
941 differentially regulate cell-cell junctions and focal adhesions. *Sci Rep* **6**, 35956 (2016).
942 35. M. M. Keenen *et al.*, Comparative analysis of the syncytiotrophoblast in placenta tissue
943 and trophoblast organoids using snRNA sequencing. *bioRxiv*, (2024).
944 36. S. J. Coleman *et al.*, Syncytial nuclear aggregates in normal placenta show increased
945 nuclear condensation, but apoptosis and cytoskeletal redistribution are uncommon.
946 *Placenta* **34**, 449-455 (2013).
947 37. M. Wang *et al.*, Single-nucleus multi-omic profiling of human placental
948 syncytiotrophoblasts identifies cellular trajectories during pregnancy. *Nat Genet* **56**, 294-
949 305 (2024).
950 38. C. Xu *et al.*, Probabilistic harmonization and annotation of single-cell transcriptomics data
951 with deep generative models. *Mol Syst Biol* **17**, e9620 (2021).
952 39. A. Liberzon *et al.*, The Molecular Signatures Database (MSigDB) hallmark gene set
953 collection. *Cell Syst* **1**, 417-425 (2015).
954 40. W. J. Bakker, I. S. Harris, T. W. Mak, FOXO3a is activated in response to hypoxic stress
955 and inhibits HIF1-induced apoptosis via regulation of CITED2. *Mol Cell* **28**, 941-953
956 (2007).
957 41. B. Brandstetter *et al.*, FOXO3 is involved in the tumor necrosis factor-driven
958 inflammatory response in fibroblast-like synoviocytes. *Lab Invest* **99**, 648-658 (2019).
959 42. D. R. Premkumar *et al.*, Intracellular pathways linking hypoxia to activation of c-fos and
960 AP-1. *Adv Exp Med Biol* **475**, 101-109 (2000).
961 43. N. Ray *et al.*, c-Fos suppresses systemic inflammatory response to endotoxin. *Int Immunol*
962 **18**, 671-677 (2006).

963 44. T. Jansson, M. Wennergren, N. P. Illsley, Glucose transporter protein expression in human
964 placenta throughout gestation and in intrauterine growth retardation. *J Clin Endocrinol*
965 *Metab* **77**, 1554-1562 (1993).
966 45. C. N. Lok, P. Ponka, Identification of a hypoxia response element in the transferrin
967 receptor gene. *J Biol Chem* **274**, 24147-24152 (1999).
968 46. M. Uhlen *et al.*, The human secretome. *Sci Signal* **12**, (2019).
969 47. I. Brosens, R. Pijnenborg, L. Vercruysse, R. Romero, The "Great Obstetrical Syndromes"
970 are associated with disorders of deep placentation. *Am J Obstet Gynecol* **204**, 193-201
971 (2011).
972 48. Y. Yu *et al.*, Placensin is a glucogenic hormone secreted by human placenta. *Embo Rep* **21**,
973 e49530 (2020).
974 49. R. Rojas-Rodriguez *et al.*, PAPPA-mediated adipose tissue remodeling mitigates insulin
975 resistance and protects against gestational diabetes in mice and humans. *Sci Transl Med*
976 **12**, (2020).
977 50. P. Sedlmayr, A. Blaschitz, R. Stocker, The role of placental tryptophan catabolism. *Front*
978 *Immunol* **5**, 230 (2014).
979 51. A. Winship *et al.*, Blocking Endogenous Leukemia Inhibitory Factor During Placental
980 Development in Mice Leads to Abnormal Placentation and Pregnancy Loss. *Sci Rep* **5**,
981 13237 (2015).
982 52. Z. Wang *et al.*, Acetylcholine ameliorated hypoxia-induced oxidative stress and apoptosis
983 in trophoblast cells via p38 MAPK/NF-kappaB pathway. *Mol Hum Reprod* **27**, (2021).
984 53. S. Sato, N. Fujita, T. Tsuruo, Modulation of Akt kinase activity by binding to Hsp90. *Proc*
985 *Natl Acad Sci U S A* **97**, 10832-10837 (2000).
986 54. R. E. Leach, B. A. Kilburn, A. Petkova, R. Romero, R. Armant, Diminished survival of
987 human cytotrophoblast cells exposed to hypoxia/reoxygenation injury and associated
988 reduction of heparin-binding epidermal growth factor-like growth factor. *American*
989 *Journal of Obstetrics and Gynecology* **198**, (2008).
990 55. A. Lachmann *et al.*, Massive mining of publicly available RNA-seq data from human and
991 mouse. *Nature Communications* **9**, (2018).
992 56. J. X. Binder *et al.*, COMPARTMENTS: unification and visualization of protein
993 subcellular localization evidence. *Database-Oxford*, (2014).
994 57. M. Shibuya, Vascular endothelial growth factor receptor-1 (VEGFR-1/Flt-1): a dual
995 regulator for angiogenesis. *Angiogenesis* **9**, 225-230; discussion 231 (2006).
996 58. C. Cursiefen *et al.*, VEGF-A stimulates lymphangiogenesis and hemangiogenesis in
997 inflammatory neovascularization via macrophage recruitment. *J Clin Invest* **113**, 1040-
998 1050 (2004).
999 59. L. A. Dyer, S. Rugonyi, Fetal Blood Flow and Genetic Mutations in Conotruncal
1000 Congenital Heart Disease. *J Cardiovasc Dev Dis* **8**, (2021).
1001 60. H. Wu, K. Liu, J. Zhang, Excess fibronectin 1 participates in pathogenesis of pre-
1002 eclampsia by promoting apoptosis and autophagy in vascular endothelial cells. *Mol Hum*
1003 *Reprod* **27**, (2021).
1004 61. T. Chen *et al.*, Sphingosine-1-phosphate derived from PRP-Exos promotes angiogenesis in
1005 diabetic wound healing via the S1PR1/AKT/FN1 signalling pathway. *Burns Trauma* **11**,
1006 tkad003 (2023).
1007 62. A. S. Zannas *et al.*, Epigenetic upregulation of FKBP5 by aging and stress contributes to
1008 NF-κB-driven inflammation and cardiovascular risk. *P Natl Acad Sci USA* **116**, 11370-
1009 11379 (2019).
1010 63. S. Ognjanovic, G. D. Bryant-Greenwood, Pre-B-cell colony-enhancing factor, a novel
1011 cytokine of human fetal membranes. *American Journal of Obstetrics and Gynecology* **187**,
1012 1051-1058 (2002).

1013 64. L. Zernichow *et al.*, Serglycin is the major secreted proteoglycan in macrophages and has
1014 a role in the regulation of macrophage tumor necrosis factor-α secretion in response to
1015 lipopolysaccharide. *J Biol Chem* **281**, 26792-26801 (2006).
1016 65. T. P. J. Hofer *et al.*, Tissue-specific induction of ADAMTS2 in monocytes and
1017 macrophages by glucocorticoids. *J Mol Med* **86**, 323-332 (2008).
1018 66. C. C. Campa, E. Ciraolo, A. Ghigo, G. Germena, E. Hirsch, Crossroads of PI3K and Rac
1019 pathways. *Small GTPases* **6**, 71-80 (2015).
1020 67. X. B. Zhang, N. M. Tang, T. J. Hadden, A. K. Rishi, Akt, FoxO and regulation of
1021 apoptosis. *Bba-Mol Cell Res* **1813**, 1978-1986 (2011).
1022 68. M. Alikhani, Z. Alikhani, D. T. Graves, FOXO1 functions as a master switch that regulates
1023 gene expression necessary for tumor necrosis factor-induced fibroblast apoptosis. *J Biol*
1024 *Chem* **280**, 12096-12102 (2005).
1025 69. D. Dimitrov *et al.*, LIANA plus provides an all-in-one framework for cell-cell
1026 communication inference. *Nat Cell Biol*, (2024).
1027 70. V. Audrito, V. G. Messana, S. Deaglio, NAMPT and NAPRT: Two Metabolic Enzymes
1028 With Key Roles in Inflammation. *Front Oncol* **10**, (2020).
1029 71. M. L. Corcoran, W. G. Stetler-Stevenson, Tissue inhibitor of metalloproteinase-2
1030 stimulates fibroblast proliferation via a cAMP-dependent mechanism. *J Biol Chem* **270**,
1031 13453-13459 (1995).
1032 72. T. Maruo, H. Matsuo, K. Murata, M. Mochizuki, Gestational Age-Dependent Dual Action
1033 of Epidermal Growth-Factor on Human Placenta Early in Gestation. *J Clin Endocr Metab*
1034 **75**, 1362-1367 (1992).
1035 73. M. Faxén, J. Nasiell, A. Blanck, H. Nisell, N. O. Lunell, Altered mRNA expression pattern
1036 of placental epidermal growth factor receptor (EGFR) in pregnancies complicated by
1037 preeclampsia and/or intrauterine growth retardation. *Am J Perinat* **15**, 9-13 (1998).
1038 74. R. Z. Shafagh *et al.*, Bioengineered Pancreas-Liver Crosstalk in a Microfluidic Coculture
1039 Chip Identifies Human Metabolic Response Signatures in Prediabetic Hyperglycemia. *Adv*
1040 *Sci* **9**, (2022).
1041 75. J. X. Shen *et al.*, 3D Adipose Tissue Culture Links the Organotypic Microenvironment to
1042 Improved Adipogenesis. *Adv Sci* **8**, (2021).
1043 76. M. Y. Turco *et al.*, Trophoblast organoids as a model for maternal-fetal interactions during
1044 human placentation. *Nature* **564**, 263-+ (2018).
1045 77. L. Yang *et al.*, Innate immune signaling in trophoblast and decidua organoids defines
1046 differential antiviral defenses at the maternal-fetal interface. *Elife* **11**, (2022).
1047 78. N. M. Warrington *et al.*, Maternal and fetal genetic effects on birth weight and their
1048 relevance to cardio-metabolic risk factors. *Nat Genet* **51**, 804-+ (2019).
1049 79. S. Vogelezang *et al.*, Novel loci for childhood body mass index and shared heritability
1050 with adult cardiometabolic traits. *Plos Genet* **16**, (2020).
1051 80. C. A. de Leeuw, J. M. Mooij, T. Heskes, D. Posthuma, MAGMA: Generalized Gene-Set
1052 Analysis of GWAS Data. *Plos Comput Biol* **11**, (2015).
1053 81. S. W. Zhang, A simplified protocol for performing MAGMA/ H-MAGMA gene set
1054 analysis utilizing high-performance computing environments. *Star Protoc* **3**, (2022).
1055 82. B. Bhaumick, D. George, R. M. Bala, Potentiation of Epidermal Growth Factor-Induced
1056 Differentiation of Cultured Human Placental Cells by Insulin-Like Growth Factor-I. *J Clin*
1057 *Endocr Metab* **74**, 1005-1011 (1992).
1058 83. N. Jansson *et al.*, Maternal hormones linking maternal body mass index and dietary intake
1059 to birth weight. *Am J Clin Nutr* **87**, 1743-1749 (2008).
1060 84. A. Varastehpour *et al.*, \Activation of phospholipase A2 is associated with generation of
1061 placental lipid signals and fetal obesity. *J Clin Endocr Metab* **91**, 248-255 (2006).
1062 85. A. Zhao *et al.*, Appropriate glycemic management protects the germline but not the uterine

1063 environment in hyperglycemia. *Embo Rep* **25**, 1752-1772 (2024).
1064 86. J. E. Ramsay *et al.*, Maternal obesity is associated with dysregulation of metabolic,
1065 vascular, and inflammatory pathways. *J Clin Endocrinol Metab* **87**, 4231-4237 (2002).
1066 87. T. Kawai, M. V. Autieri, R. Scalia, Adipose tissue inflammation and metabolic dysfunction
1067 in obesity. *Am J Physiol Cell Physiol* **320**, C375-C391 (2021).
1068 88. P. Zhang, J. Miska, A. B. Heimberger, GLUT3 regulates alternative macrophage signaling
1069 through a glucose transport-independent role. *J Clin Invest* **133**, (2023).
1070 89. R. Bill *et al.*, CXCL9:SPP1 macrophage polarity identifies a network of cellular programs
1071 that control human cancers. *Science* **381**, 515-524 (2023).
1072 90. R. E. Bezemer, M. M. Faas, H. van Goor, S. J. Gordijn, J. R. Prins, Decidual macrophages
1073 and Hofbauer cells in fetal growth restriction. *Front Immunol* **15**, (2024).
1074 91. J. Loegl *et al.*, Hofbauer cells of M2a, M2b and M2c polarization may regulate feto-
1075 placental angiogenesis. *Reproduction* **152**, 447-455 (2016).
1076 92. A. D. Goudreau, C. Everest, L. Tanara, V. Tzaneva, K. B. Adamo, Characterization of
1077 Hofbauer cell polarization and VEGF localization in human term placenta from active and
1078 inactive pregnant individuals. *Physiological Reports* **11**, (2023).
1079 93. R. Hashimoto, K. Sakai, H. Matsumoto, M. Iwashita, Tumor Necrosis Factor-α (TNF-α)
1080 Inhibits Insulin-like Growth Factor-I (IGF-I) Activities in Human Trophoblast Cell
1081 Cultures Through IGF-I/Insulin Hybrid Receptors. *Endocr J* **57**, 193-200 (2010).
1082 94. K. Hoeft *et al.*, Platelet-instructed SPP1(+) macrophages drive myofibroblast activation in
1083 fibrosis in a CXCL4-dependent manner. *Cell Rep* **42**, 112131 (2023).
1084 95. F. A. Wolf, P. Angerer, F. J. Theis, SCANPY: large-scale single-cell gene expression data
1085 analysis. *Genome Biology* **19**, (2018).
1086 96. S. J. Fleming *et al.*, Unsupervised removal of systematic background noise from droplet-
1087 based single-cell experiments using CellBender. *Nat Methods* **20**, 1323-+ (2023).
1088 97. S. L. Wolock, R. Lopez, A. M. Klein, Scrublet: Computational Identification of Cell
1089 Doublets in Single-Cell Transcriptomic Data. *Cell Syst* **8**, 281-+ (2019).
1090 98. K. Street *et al.*, Slingshot: cell lineage and pseudotime inference for single-cell
1091 transcriptomics. *Bmc Genomics* **19**, 477 (2018).
1092 99. , (!!! INVALID CITATION !!! 20).
1093 100. M. Buttner, J. Ostner, C. L. Muller, F. J. Theis, B. Schubert, scCODA is a Bayesian model
1094 for compositional single-cell data analysis. *Nat Commun* **12**, 6876 (2021).
1095 101. A. Butler, P. Hoffman, P. Smibert, E. Papalexi, R. Satija, Integrating single-cell
1096 transcriptomic data across different conditions, technologies, and species. *Nat Biotechnol*
1097 **36**, 411-+ (2018).
1098 102. A. Subramanian *et al.*, Gene set enrichment analysis: a knowledge-based approach for
1099 interpreting genome-wide expression profiles. *Proc Natl Acad Sci U S A* **102**, 15545-
1100 15550 (2005).
1101 103. Y. Benjamini, Y. Hochberg, Controlling the False Discovery Rate - a Practical and
1102 Powerful Approach to Multiple Testing. *J R Stat Soc B* **57**, 289-300 (1995).
1103 104. D. Dimitrov *et al.*, LIANA plus provides an all-in-one framework for cell-cell
1104 communication inference. *Nat Cell Biol* **26**, (2024).
1105 105. A. Janjic *et al.*, Prime-seq, efficient and powerful bulk RNA sequencing. *Genome Biol* **23**,
1106 88 (2022).
1107 106. S. Parekh, C. Ziegenhain, B. Vieth, W. Enard, I. Hellmann, zUMIs - A fast and flexible
1108 pipeline to process RNA sequencing data with UMIs. *Gigascience* **7**, (2018).
1109 107. A. Dobin *et al.*, STAR: ultrafast universal RNA-seq aligner. *Bioinformatics* **29**, 15-21
1110 (2013).
1111 108. Y. Liao, G. K. Smyth, W. Shi, The R package Rsubread is easier, faster, cheaper and better
1112 for alignment and quantification of RNA sequencing reads. *Nucleic Acids Res* **47**, e47

(2019).